Mol Neurobiol
DOI 10.1007/s12035-017-0589-0

Cytoskeleton-Associated Risk Modifiers Involved in Early and Rapid Progression of Sporadic Creutzfeldt-Jakob Disease

Saima Zafar[1] · Neelam Younas[1] · Nadeem Sheikh[2] · Waqas Tahir[1] · Mohsin Shafiq[1] · Matthias Schmitz[1] · Isidre Ferrer[3,4] · Olivier Andréoletti[5] · Inga Zerr[1]

Received: 19 January 2017 / Accepted: 28 April 2017

Abstract A high priority in the prion field is to identify pre-symptomatic events and associated profile of molecular changes. In this study, we demonstrate the pre-symptomatic dysregulation of cytoskeleton assembly and its associated cofilin-1 pathway in strain and brain region-specific manners in MM1 and VV2 subtype-specific Creutzfeldt-Jakob disease at clinical and pre-clinical stage. At physiological level, PrP^C interaction with cofilin-1 and phosphorylated form of cofilin (p-cofilin(Ser3)) was investigated in primary cultures of mouse cortex neurons (PCNs) of PrP^C wild-type and knockout mice ($PrP^{-/-}$). Short-interfering RNA downregulation of active form of cofilin-1 resulted in the redistribution/downregulation of PrP^C, increase of activated form of microglia, accumulation of dense form of F-actin, and upregulation of p-cofilin(Ser3). This upregulated p-cofilin(Ser3) showed redistribution of expression predominantly in the activated form of microglia in PCNs. At pathological level, cofilin-1 expression was significantly altered in cortex and cerebellum in both humans and mice at pre-clinical stage and at early symptomatic clinical stage of the disease. Further, to better understand the possible mechanism of dysregulation of cofilin-1, we also demonstrated alterations in upstream regulators; LIM kinase isoform 1 (LIMK1), slingshot phosphatase isoform 1 (SSH1), RhoA-associated kinase (Rock2), and amyloid precursor protein (APP) in sporadic Creutzfeldt-Jakob disease MM1 mice and in human MM1 and VV2 frontal cortex and cerebellum samples. In conclusion, our findings demonstrated for the first time a key pre-clinical response of cofilin-1 and the associated pathway in prion disease.

Saima Zafar and Neelam Younas have equal contributions.

Significance Statement In prion field, a high demand is arising to uncover pre-clinical events and the alteration of associated pathway as the clinical stage is much squatter than pre-clinical stage. For public health concern, early diagnosis is a big need as the disease can be transmitted by blood. So, if the blood donors had prion disease in a pre-clinical stage, and the prion disease was diagnosed at a later date, this could be a risk for public health and a concern to develop diagnostic tools by studying early pre-clinical molecular pathways. To address this need, targeting cofilin-1 activity in LIMK-APP-SSH1 signaling pathways might be a promising strategy to study the most likely disease progression and the internal homeostasis of misfolded proteins.

✉ Saima Zafar
sz_awaan@yahoo.com; saima.zafar@med.uni-goettingen.de

[1] Department of Neurology, Clinical Dementia Center, and DZNE, Georg-August University, University Medical Center Goettingen (UMG), Robert-Koch-Str. 40, 37075 Goettingen, Germany

[2] Department of Zoology, University of the Punjab, Lahore, Pakistan

[3] Institute of Neuropathology, IDIBELL—University Hospital Bellvitge, University of Barcelona, Hospitalet de Llobregat, Spain

[4] Network Center for Biomedical Research of Neurodegenerative Diseases (CIBERNED), Institute Carlos III, Ministry of Health, Madrid, Spain

[5] Institut National de la Recherche Agronomique/Ecole Nationale Vétérinaire, Toulouse, France

Published online: 01 June 2017

Keywords Cofilin · Actin · CJD · MM1 · VV2 · Prion protein · LIMK · Rock · APP · SSH1 · Microglia · Cerebellum · Cortex

Introduction

Sporadic Creutzfeldt-Jakob disease (sCJD) is the most common form of prion diseases in humans [1]. Based on pathological form of prion protein (PrP^{Sc}) electrophoretic mobility and allelic variation at codon 129, sCJD has been divided into six subtypes [2–4] among which sCJD MM1 and sCJD VV2 are the two most commonly occurring subtypes [3]. Although clinico-pathological features of the molecular disease subtypes differ markedly by the affected brain area, severity, and morphological features; but spongiform degeneration or severe gliosis, neuronal loss, and dysfunction are critical and constant features of CJD [5]. Synaptic loss and degeneration of the axon terminal are early abnormalities in experimental scrapie [6, 7]. Indeed, accumulation of pathological form (PrP^{Sc}) of prion triggers a pathological mechanism leading to synaptic abnormalities [5]. Recently, a role of PrP^{C} in control of neurite sprouting and dendritic spine formation has been described through the modulation of actin dynamics [8, 9].

Actin cytoskeleton is crucial for neurite growth cone, spine development, and formation of synapses in neurons [10–12]. Perfect balance in remodeling of actin is required for maturation and maintenance of the synapses by regulating spine morphology [13–17]. In mammals, the actin-depolymerizing factor (ADF)/cofilin family of proteins, consisting of cofilin-1 (a non-muscle type), cofilin-2 (a muscle-type), and ADF (also known as destrin), is the major and critical regulator of actin dynamics and reorganization by depolymerization and severing of actin filaments [18–20]. A growing body of evidence provides support to a link between neurite transportation abnormalities and synaptic plasticity impairment observed in neurodegenerative diseases [21], as well as alterations in the organization and dynamics of the actin cytoskeleton initiated by cofilin-1 [19, 22–25]. The regulatory response of cofilin-1 activity is quite complex and is maintained by a cohort of kinases and phosphatases [26]. In particular, cofilin-1 is inactivated by LIM kinase isoform 1 (LIMK1)-mediated phosphorylation at serine 3 (Ser3) that halts its actin binding activity, and dephosphorylation by slingshot phosphatase isoform 1 (SSH1), reactivates cofilin-1 [19, 25, 27–29]. Although other kinases and phosphatases can also affect cofilin-1 activity, LIMK1 and SSH1 show the highest substrate specificity [26]. Remarkably, phosphorylation of LIMK1 at threonine 505 and 508 activates it, and phosphorylation at serine 937 and 978 inactivates SSH1 [30]. Further, not only cofilin-1 but also LIMK1 is dephosphorylated by SSH1 activity. So, SSH1 can control cofilin-1 activity either directly or indirectly through an upstream regulation of LIMK1 [30]. Moreover, SSH1 is also a potential interactor of 14-3-3 protein [31], and 14-3-3 is known to be markedly elevated in the CSF of CJD patients [32–34].

In this study, our main objective was to uncover molecular changes in cofilin-LIMK pathway, a major regulator of actin dynamics, in two most frequent subtypes of sCJD (MM1 and VV2) and in a mouse model at pre-symptomatic and symptomatic stages of the disease. Interaction between PrP^{C} and cofilin-1, as well as its phosphorylated form, was investigated in cellular model. This study demonstrated that regulation of cofilin-LIMK pathway is altered in sCJD in a brain region- and subtype-specific manner. Remarkably, dysregulation of cofilin-LIMK pathway at pre-symptomatic stage of the disease signifies events initiated early in the pathological cascade. Meanwhile, translation study in primary cultures of mouse cortex neurons (PCNs) demonstrated the functional aspect of cofilin-1 depletion on actin dynamics, microglial activation, and upregulation/redistribution of phosphorylated form of cofilin at clinical stage of the disease in humans. Further differential manifestation/regulation of cofilin-LIMK pathway in both subtypes of sCJD provides potential new insights into the molecular mechanisms involved in pathology and heterogeneity of prion diseases.

Materials and Methods

Ethics Statement

Human samples from the Institute of Neuropathology Brain Bank (HUB-ICO-IDIBELL Biobank) and Biobank of Hospital Clinic-IDIBAPS were obtained following the Spanish legislation (Ley de la Investigación Biomédica 2013 and Real DecretoBiobancos 2014) and the approval of the local ethics committees.

All animal experiments were performed in accordance with the ethical standard set by Regierungspräsidium Tübingen (Regional Council) Experimental No. FLI 231/07 file reference number 35/9185.81-2. All animal experiments have been performed in compliance with the institutional and French national guidelines, in accordance with the European Community Council Directive 86/609/EEC. The experimental protocol was approved by the INRA Toulouse/ENVT ethics committee.

CJD Patients, Samples Processing, and Subtype Characterization

In this study, 30 pathologically confirmed sCJD patient's brain tissue samples, i.e., frontal cortex and cerebellum regions (15 of each MM1 and VV2 subtypes) and 15 age-matched control cases (CON) were analyzed. All 45 samples were obtained from the Institute of Neuropathology Brain Bank (HUB-ICO-IDIBELL Biobank) and Biobank of Hospital Clinic-

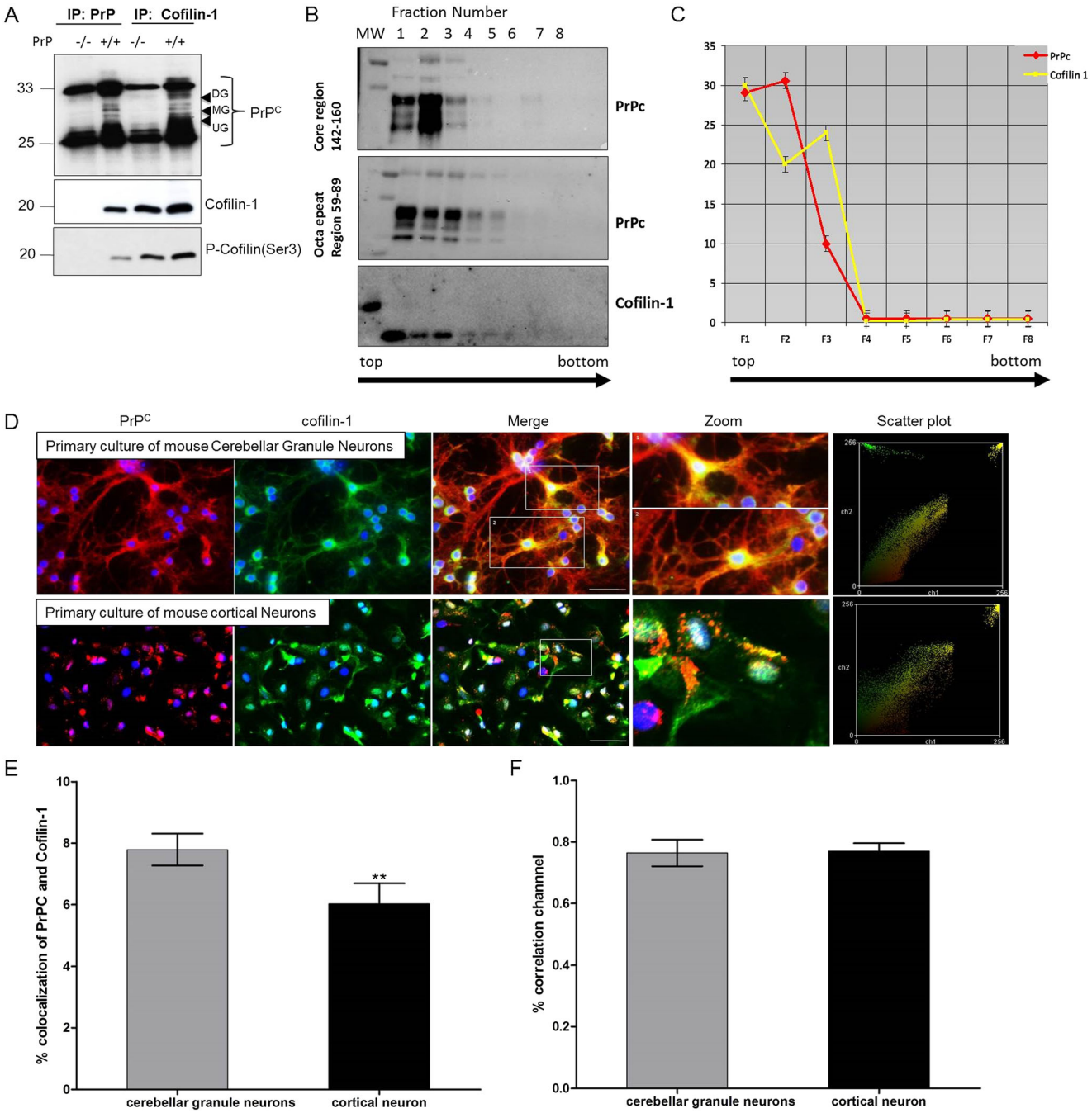

Fig. 1 Interactive association between PrP^C and cofilin-1. Primary cultures of mouse cortex neurons (PCNs) encoding PrP gene and knockout ($PrP^{-/-}$) were prepared from pregnant mice at embryonic day 14. **a** Total cellular lysate co-immunoprecipitated (IP) with PrP^C antibody (lane 1 $PrP^{-/-}$ PCNs and lane 2 PrP^C-expressing PCNs); cofilin-1 antibody (lane 3 $PrP^{-/-}$ PCNs and lane 4 PrP^C-expressing PCNs); and then immunoblotted with SAF70 PrP^C, cofilin-1, and p-cofilin(Ser3) antibodies. **b**, **c** Western blot with PrP^C and cofilin-1 from fractions isolated after ultracentrifugation using sucrose step gradient. Densitometry analysis from four independent (±SD) sedimentation ultracentrifugation fractionation experiments. **d** PrP^C and cofilin-1 distribution was analyzed in primary cultures of mouse cerebellar granule neurons (PCGNs) and primary mouse corticle neurons (PCNs) using 3F4 anti-PrP^C (*red*), anti-cofilin-1 (*green*) antibodies, and DAPI (*blue*-nuclear staining). At least 35 cells were observed per condition per experiment for an equal exposure time (*Scale bar* 10 μm). The co-localization scatter frequency plots of the individual pixels from paired images and co-localization frequency graphs were generated by ImageJ (WCIF plugin) software. **e**, **f** Pearson's colocalization correlation coefficient rp ($-1 \leq rp \leq 1$) showed % co-localization and % correlation btween PrP^C and cofilin-1 in cerebellar granule neuron and in cortical neurons. Graph was generated by ImageJ (WCIF plugin) software

IDIBAPS. The mean age and gender of study cases were as described previously [35, 36]. In brief, for sCJD frontal cortex, 60 years of mean age in control (10M/5F), 68 years of mean age in sCJD MM1 (10M/5F), and 63 years of mean age in

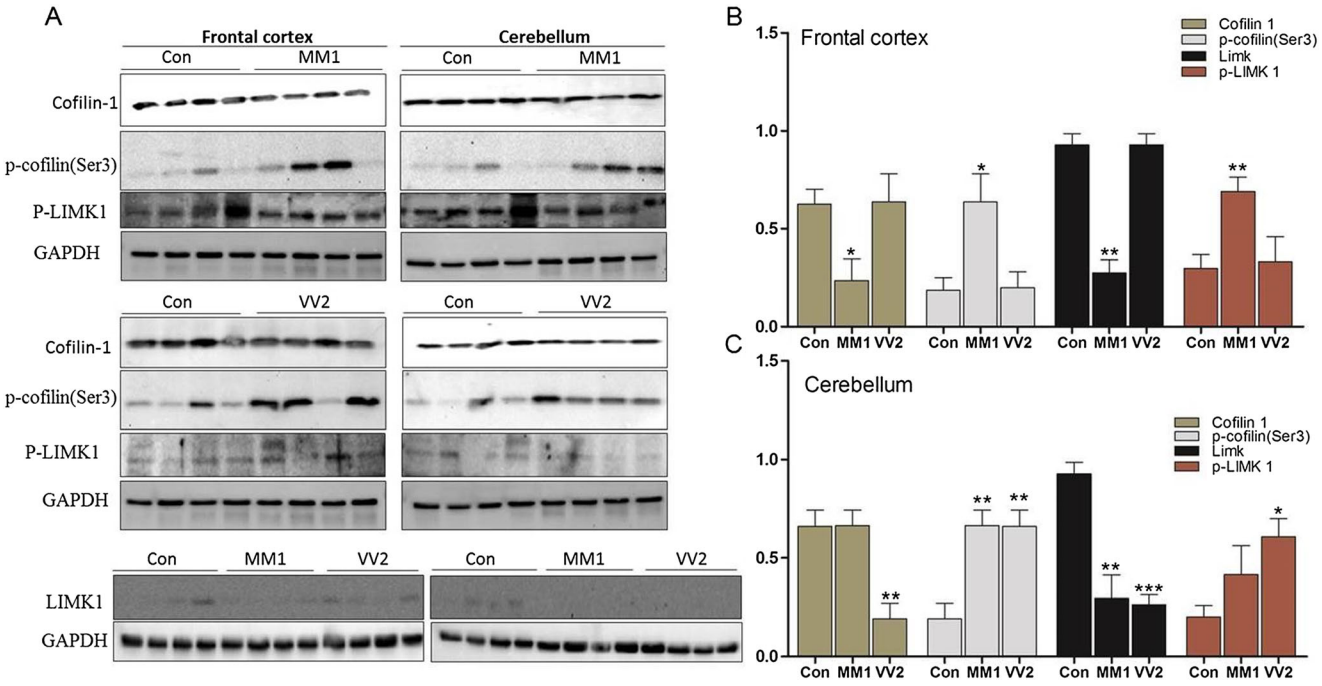

Fig. 2 Cofilin-1, p-cofilin(Ser3), LIMK1, and P-LIMK1 expressions in sCJD MM1 and VV2 subtypes. Western blotting analysis: **a** cofilin-1, p-cofilin(Ser3), LIMK1, and P-LIMK1 in four representative cases each for control, sCJD MM1, and sCJD VV2 cases; GAPDH immunostaining was used to normalize total protein loading. **b**, **c** Densitometry analysis from four independent (±SD) immunoblotting experiments of 15 control (Con), 15 MM1, and 15 VV2 cases. The significance was calculated with one-way ANOVA Friedman test (*$P < 0.05$, **$P < 0.01$, ***$P < 0.001$). *AU* arbitrary units

sCJD VV2 (5 M/10F). In cerebellum, the mean age was 62 years in control (11M/4F), 66 years of mean age in sCJD MM1 (10M/5F), and 63 years of mean age in sCJD VV2 (4M/10F). After post-mortem interval ranging 1 h 45 min to 24 h 30 min, coronal sections 1 cm thick were cut from one of the hemispheres. Along with selectively dissected areas of encephalon, coronal sections were rapidly frozen on metal plates over dry ice, sorted in separate bags, labeled with water-resistant ink and stored at −80 °C until further use for biochemical investigations. The other hemisphere was fixed in 4% buffered formalin for 3 weeks for morphological studies and neuropathological examination and characterization. The analysis of the codon 129 genotype of PrP gene (Met: M or Val: V) was performed after isolation of genomic DNA from blood samples according to standard methods. Western blot profile of PrP^{Sc} was classified as type 1 or type 2 based on electrophoretic mobility after proteinase K (PK) digestion.

sCJD MM1 and VV2 Transgenic Mice

Double transgenic Tg340 mice overexpressing about 4-fold level of human PrP^{C} with methionine at codon 129 (Met129 and Val129) on a murine PrP knockout background were used, as described previously [9, 36, 37]. Inocula were prepared from sCJD MM1 and VV2 brain tissues as 10% (*w*/*v*) homogenates. Individually identified 6- to 10-week-old mice were anesthetized and inoculated with 2 mg of brain homogenate in the right parietal lobe using a 25-gauge disposable hypodermic needle (six animals per group and time point). Mice were observed daily, and the neurological status was assessed weekly. When disease progression was evident, or at the end of lifespan, animals were euthanized, necropsy was performed, and the brain was removed. A part of the brain was fixed by immersion in 10% buffered formalin to quantify spongiform degeneration and perform immunohistological procedures. The other part was frozen at −80 °C to extract protein. Survival time was calculated for each isolate and expressed as the mean of the survival day post-inoculation (dpi) of all mice scoring positive for PrP^{Sc}. Infection rate was determined as the proportion of mice scoring positive for PrP^{Sc} from all inoculated mice.

Primary Culture of Mouse Cortex, Cerebellum, Gene Manipulation, Transfection, and RNAi

PCNs and cerebellum (PCE) were prepared as described previously [36, 38]. In brief, embryos were removed from pregnant mice at embryonic day 14 under halothane (Sigma) anesthesia; the mice were *prnp* (the PrP-encoding gene) and knockout ($PrP^{-/-}$) [39]. Animals were killed by cervical dislocation and the dissected embryonic cortex was mechanically dissociated and plated on polyethylenimine (1 mg/ml)-coated glass coverslips in culture wells.

After 3 days in vitro (DIV), the medium was replaced with N5 medium [40] with 180 mg/L glucose and supplemented with 5% FBS and 1% FCS. Three micromolars of cytosine arabinoside was added to prevent astrocyte proliferation (resulting in at least 97% pure neuronal cultures) and 1 μM MK-801 to prevent excitotoxicity [41]. The medium was changed daily. On DIV 5, FCS was removed and the FBS content was reduced to 1%.

The cells were seeded in complete DMEM prior to transient transfection with plasmid and short-interfering RNA (siRNA) duplexes using Lipofectamine 2000 (Invitrogen, Carlsbad, CA, USA) according to the manufacturer's instructions. Cofilin-1 siRNA duplex had a sense strand 5′-GGAG GACCUGGUGUUCAUC-3′ [42], and non-targeting siRNA duplex (control siRNA duplex negative control: Eurogentec) [9] was used as a negative control.

Assessment of Neuronal/Cell Viability and Caspase-3 Activity Assay

The viability of neurons in primary cortical cultures, with and without depletion of cofilin-1 and in the presence of PrP^C, was checked by counting number of healthy nuclei per unit area after Hoechst staining. The identification of individual neuron viability that was unequivocally healthy on the basis of its nuclear appearance using a combination of fluorescent illumination and phase contrast [43].

Cell viability assay was performed as described previously [44]. Briefly, the adherent cells were grown up to 60–70% confluency and then detached from flasks using 1× Trypsin-EDTA. The cells were spun down at 4 °C for 5 min at 400×*g* and resuspended in culture media. Cells were then dispensed into 24-well plates (Nunc, Roskilde, Denmark) at a final concentration of 1×10^5 cells/well and incubated for 12 h. The culture media were then removed and replaced prior to MTS [3-(4,5-dimethylthiazol-2-yl)-5-(3-carboxymethoxyphenyl)-2-(4-sulfophenyl) 2H-tetrazolium, inner salt] treatment. The effect of the presence of PrP^C and the treatment of TNF-alpha on cell viability was measured using the MTS cell proliferation assay, which measures the reduction of MTS tetrazolium salt to formazan in metabolically active cells [45]. The cells were then treated with 1:20 ratio of MTS reagent (Promega Co. Madison, WI, USA) 2 mg/ml with 0.5% glucose and PMS 0.92 mg/ml with 0.5% glucose. Cells were incubated for 1 h at 37 °C for color development, and the absorbance values were read at 490 nm using a Multiscan Plate Reader (Labsystems, VA, USA) and Accent software 2.6. Background absorbance from controls was incubated in media with the MTS reagent and was subtracted from sample wells after the final absorbance was obtained.

The caspase-3-activity assay allows quantitative measurement of caspase-3 (DEVDase) protease activity, which is an early regulatory event in the apoptotic cell death process. The assay was performed using caspase-3 activity assay kit according to the manufacturer's recommendations. Briefly, cofilin-1 depleted PCNs were lysed in the cell lysis buffer for 15 min at 4 °C, and this was followed by centrifugation at 10,000×*g*. Protein concentration was estimated from the supernatants, and the total cell lysate (50 μg) was then incubated with 50 μM caspase-caspase-3-specific substrate DEVD-pNA (Asp-Glu-Val-Asp p-nitroanilide) for 4-5 h at 37 °C. The caspase-3 inhibitor Z-vad-FMK (20 μM) was used as control. Caspase-3-mediated release of pNA was measured by absorbance at 405 nm. Background absorbance from the control (untreated cells) was subtracted from the samples after the final absorbance was obtained.

Co-sedimentation Assay

Two hundred microliters of 10% brain homogenate in PBS containing 2% *w*/*v* sarkosyl (pH 7.4) were clarified for 5 min at 500×*g*, and were carefully layered onto the top of 10–60% sucrose step gradient. Gradients were prepared in thin wall polyallomer tubes (11 × 34 mm, 2.2 ml, Beckman), and sucrose serial dilutions (10, 12.5, 15, 17.5, 20, 22.5, and 60%, *w*/*v*) were made in PBS containing 1% sarkosyl (pH 7.4). All the gradients in an experiment were prepared with a same batch of buffers. For avoiding mixing of sucrose serial dilutions while setting gradient in tubes, tubes (sucrose layers) were frozen for 10 min at −80 °C after adding each sucrose layer; and next layer was then added over previous frozen layer. Ultracentrifugation was performed at 55,000 rpm for 5 h at 5 °C in Optima™ TL Ultracentrifuge (Beckman Coulter) equipped with Beckman Coulter TLS-55 rotor. These conditions corresponded to RCF = 259,000×*g*, angular velocity $\omega = 5759.59$ rad/s, and *k* factor = 50. After centrifugation, 20 fractions, 100 μl each, were collected carefully from top to bottom in separate tubes and proceeded for immunoblotting.

Co-immunoprecipitation

Cell lysis was performed as described previously [9, 46], and the insoluble cell debris was removed by centrifugation at 543,000×*g* for 15 min at 4 °C. Immunoprecipitation was performed using magnetic Dynabeads protein G, according to the manufacturer's instructions. Total cytoplasmic cell extracts or immunoprecipitated proteins (corresponding to 2×10^6 cells/lane) were subjected to 12.5% 1-DE SDS-PAGE and, after transferring to polyvinylidenedifluoride membranes (Millipore), immunoblotting was performed as described above.

Co-immunofluorescence Confocal Microscopy

PCNs were platted on chambered slides [Lab-Tek™ II; Thermo Fisher Scientific (Nunc GmbH & Co. KG), Langenselbold

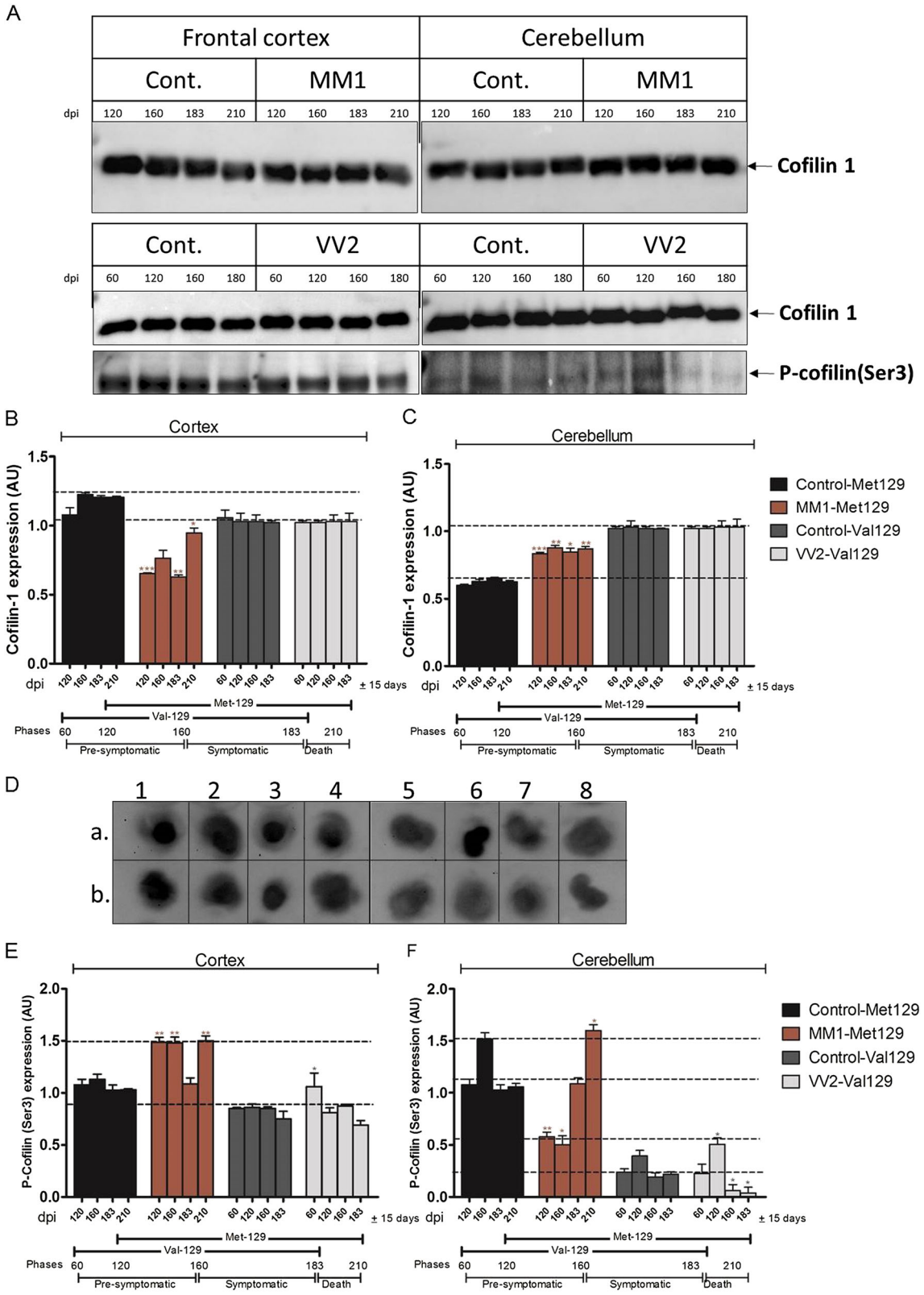

Site] and lipotransfected with cofilin-1 siRNA. Subsequently, they were washed in 1× PBS and then fixed for 15 min with 100% ethanol. After fixation, cells were permeabilized with 0.2% Triton X-100 in 1× PBS, followed by a 20-min blocking step using 0.2% casein-solution containing Tween 20. Co-localization of F-actin with cofilin-1, PrP^{C} with Iba1 and p-

◀ **Fig. 3** Expression of cofilin-1 and p-cofilin(Ser3) at pre-symptomatic and symptomatic stage of sCJD MM1 and VV2 in mice. Tg340 mice expressing about 4-fold level of human PrPM129 were infected with sCJD MM1 and also VV2 10% brain homogenates. Samples were collected at indicated days post-infection (dpi): pre-symptomatic stage (60 dpi in VV2, 120 dpi in MM1) and symptomatic stages (120–183 dpi in VV2 and 160–210 dpi). **a**, **d** Cofilin and p-cofilin(Ser3) expression in the cortex and cerebellum were observed by Western blot analysis using cofilin and p-cofilin(Ser3) antibodies. **b**, **c**, **e**, **f** Densitometry analysis from four independent (±SD) immunoblotting experiments of cofilin and p-cofilin(Ser3) from control and sCJD MM1- and VV2-infected PrPM129 mice in cortex and cerebellum. The significance was calculated with one-way ANOVA Friedman test (*$P < 0.05$)

cofilin(Ser3), and cofilin-1 with p-cofilin(Ser3) was detected by exposure to the primary antibodies [anti-PrP 3F4 (1:200), mouse anti-cofilin-1 (1:100), mouse anti-F-actin (1:100), mouse anti- p-cofilin(Ser3) (1:100)] overnight at 4 °C. The monoclonal antibodies were detected by incubating slides for 60 min with Alexa 488 conjugated anti-rabbit (1:200), Alexa 488 conjugated anti-mouse (1:200), or Cy3-labeled anti-mouse secondary antibody (1:200). Incubation with TO-PRO-3 iodide for 10 min was performed to visualize nuclei. Finally, coverslips were placed on the glass slides which were then mounted with Fluoromount (DAKO, Hamburg, Germany). All the steps were further carried out as described previously [9].

Antibodies, Reagents, and Immunoblot Analysis

Mouse anti-PrP mAb SAF32, mouse anti-PrP mAb SAF70 (1:1000; SpiBio, Paris, France), mouse anti-PrP 3F4 mAb (1:1000; Merck Millipore, Darmstadt, Germany), rabbit anti-cofilin mAb (1:1000; Sigma-Aldrich, Munich, Germany), rabbit anti-cofilin (phospho S3) mAb (1:500), mouse anti-GAPDH mAb (1:1000), mouse anti-LIM kinase 1 mAb (1:500), rabbit anti-LIM kinase 1 (phospho T508) pAb (1:500), rabbit anti-slingshot homolog 1L pAb (1:1000), rabbit anti- RhoA-associated kinase (Rock2) pAb (1:500), rabbit anti-Iba1 mAb (1:1000), mouse anti-amyloid beta A4 protein mAb (1:1000), and rabbit anti-calcineurin A mAb (1;1000) from Abcam, Cambridge, UK were used as primary antibodies. HRP-conjugated rabbit anti-mouse pAb (IBA, Goettingen, Germany), HRP-conjugated goat anti-rabbit pAb (Jackson ImmunoResearch Laboratories Europe, Ltd.), goat anti-mouse pAb cy3-conjugated (Dianova, Hamburg, Germany), anti-rabbit pAb (Santa Cruz Biotechnology, Santa Cruz, CA, USA), goat anti-rabbit (Alexa 488-conjugated), and anti-mouse (Alexa 488-conjugated) were used as secondary antibodies. Protease and phosphatase inhibitor cocktail (Roche, Mannheim, Germany), Hoechst 33342 (Sigma-Aldrich, Steinheim, Germany), halothane anesthesia, cytosine arabinoside (Sigma, St. Louis, MO, USA), MK-801 (Research Biochemicals International), penicillin, and streptomycin (Gibco) were also used.

Cell lysis and immunoblotting were performed as described previously [36, 46]. Briefly, cells were lysed (50 mM Tris-HCl, pH 8, 1% Triton X-100, 0.5% CHAPS, 1 mM DTT), and lysates were cleared of cell debris (1 min, 1000×*g*, 4 °C). Cell lysates were supplemented with protease and phosphatase inhibitors (Roche) and were separated on 12.5% 1-DE SDS-PAGE. Expression of proteins was analyzed by immunoblot using overnight exposure at 4 °C to anti-PrP SAF70 mAb (1:1000), anti-cofilin mAb (1:1000), anti-cofilin (Phospho S3) mAb (1:1000), anti-GAPDH mAb (1:1000), anti-LIM Kinase 1 mAb (1:500), anti-LIM kinase 1 (Phospho T508) pAb (1:500), anti-slingshot homolog 1L pAb (1:1000), anti-Rock2 pAb (1:500), rabbit anti-Iba1 mAb (1:1000), anti-amyloid beta A4 protein mAb (1:1000), and anti-calcineurin mAb (1;1000). Membranes were then rinsed in 1× TBS-T and incubated with the corresponding horseradish peroxidase-conjugated secondary antibody (diluted 1:2000/1:5000) for 1 h at RT. Immunoreactivity was detected after immersion of the membranes into enhanced chemiluminescence (ECL) solution and exposure to ECL-Hyperfilm (Amersham Biosciences, Buckinghamshire, UK). Images were documented using the ScanMaker4 (Microtek, International), after correction for the background, and band intensities were determined by densitometry using Lab image (version 2.7.1, Kapelan GmbH, Germany) data analyzer software.

Statistical Analysis

All results in this study were obtained from at least four independent sets of experiments and were expressed as mean ± S.D. using descriptive statistics. Densitometric analysis of 1-DE gels was performed using Labimage (version 2.7.1 Kapelan, Leipzig, Germany) software.

Results

Selective Interactive Association Between PrP^C and Cofilin-1

Previous studies have shown an interaction between PrP^C/PrP^{Sc} and cofilin-1, but the role of cofilin-1 in the pathogenesis of Prion diseases is still not clear [46, 47]. So firstly, we were interested to explore interactive association between PrP^C and cofilin-1. For this, we co-immunoprecipitated cofilin-1 from PrP^C wild-type and PrP^C knockout ($PrP^{-/-}$) primary cortical neurons (PCNs) using PrP^C antibody by Dynabeads G protein-coupled magnetic beads, and purified eluates were co-immunoblotted with SAF 70 PrP^C antibody (Fig. 1a). No signal was detected using purified eluates from

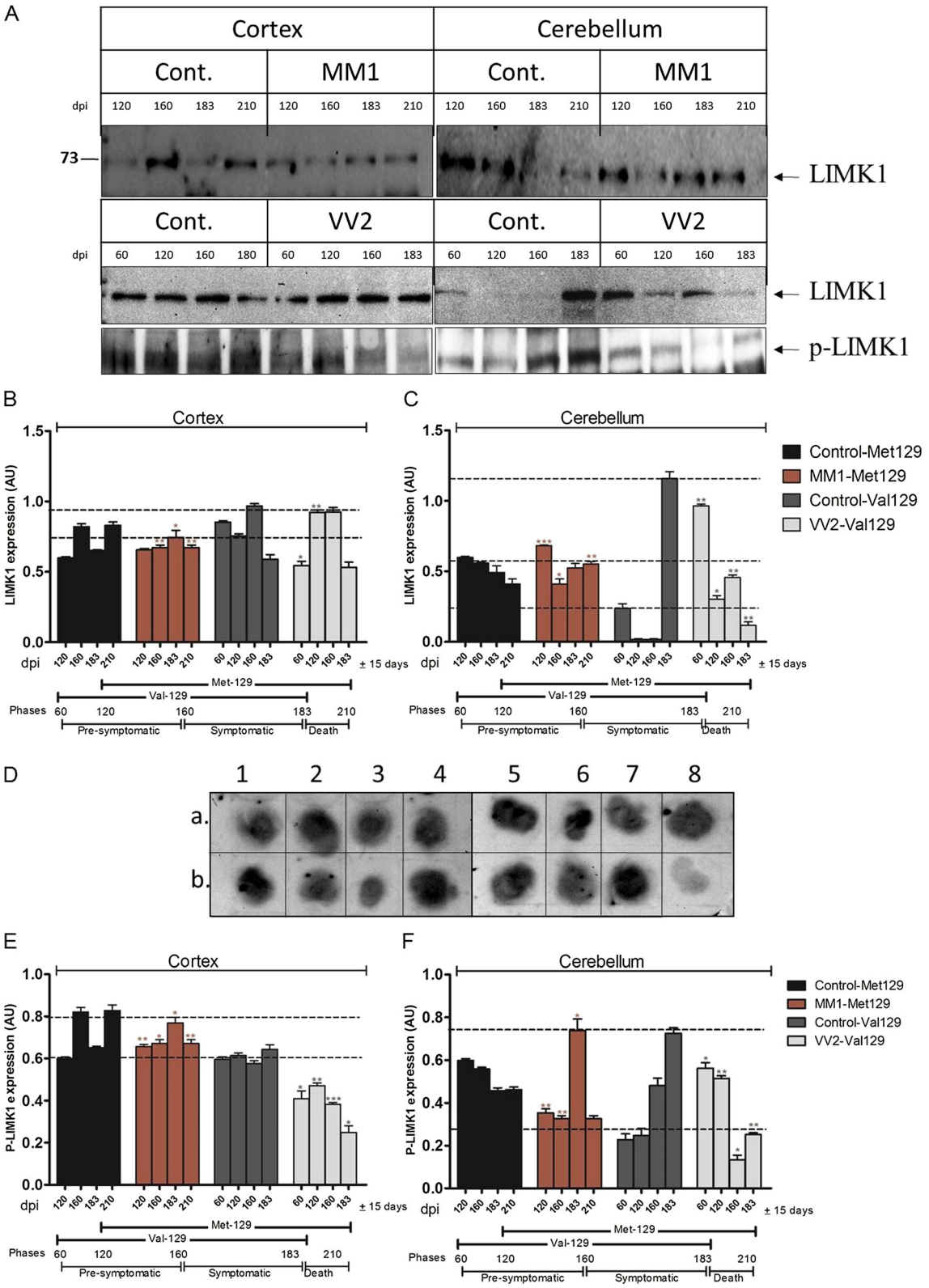

$PrP^{-/-}$ PCNs (Fig. 1a, b). In order to further confirm these observations, we co-immunoprecipitated PrP^{C} using cofilin-1 and p-cofilin antibodies (Fig. 1a). Eluates from this reverse co-immunoprecipitation were immunoblotted again with SAF70 PrP^{C} antibody to verify the PrP^{C} interaction (Fig. 1a, b). Further, PrP^{C}-expressing primary cortical cultures were co-immunoprecipitated with PrP^{C} and cofilin-1 antibodies followed by immunoblotting with anti-cofilin-1 antibody to

◀ **Fig. 4** Expression of LIMK1 and P-LIMK1 at pre-symptomatic and symptomatic stage of sCJD MM1 and VV2 in mice. Tg340 mice expressing about 4-fold level of human PrPM129 were infected with sCJD MM1 and also VV2 10% brain homogenates. Samples were collected at indicated days post-infection (dpi): pre-symptomatic stage (60 dpi in VV2, 120 dpi in MM1) and symptomatic stages (120–183 dpi in VV2 and 160–210 dpi). **a** LIMK1 and P-LIMK1 expression in the cortex and cerebellum of sCJD MM1 and VV2 in mice were observed by Western blot analysis using LIMK1 and P-LIMK1 antibodies. **d** Dot blot analysis of P-LIMK1 in the cortex and cerebellum were observed by Western blot analysis using LIMK1 and P-LIMK1 antibodies. Frontal cortex (*lane a1* = control 120 dpi, *a2* = control 160 dpi, *a3* = control 183 dpi, *a4* = control 210 dpi, *b1* = sCJD MM1-infected 120 dpi, *b2* = sCJD MM1-infected 160 dpi, *b3* = sCJD MM1-infected 183 dpi, *b4* = sCJD MM1-infected 210 dpi). Cerebellum (*lane a5* = control 120 dpi, *a6* = control 160 dpi, *a7* = control 183 dpi, *a8* = control 210 dpi; *b5* = sCJD MM1-infected 120 dpi, *b6* = sCJD MM1-infected 160 dpi, *b7* = sCJD MM1-infected 183 dpi, *b8* = sCJD MM1-infected 210 dpi). **b**, **c**, **e**, **f** Densitometry analysis from four independent (±SD) immunoblotting experiments of LIMK1 and P-LIMK1 from control and sCJD MM1- and VV2-infected PrPM129 mice in cortex and cerebellum. The significance was calculated with one-way ANOVA Friedman test (*$P < 0.05$)

confirm the interaction (Fig. 1c). Likewise, confocal laser co-immunofluorescence scanning showed region-specific co-localization of PrP^C and cofilin-1 in PCNs and in cerebellar neurons (PCB) (Fig. 1d–f). The Pearson's correlation coefficient data demonstrated significant less co-localization of PrP^C with cofilin-1 in cortical neurons as compared to cerebellar granule neurons (Fig. 1e). However, correlation channel did not show significant altered response (Fig. 1f). The interactive association between PrP^C and cofilin-1 was further verified with co-sedimentation assay at steady state and strikingly, PrP^C and cofilin-1 shared identical fractions and demonstrated the selective functional association between cofilin-1 and PrP^C (Fig. 1g, h).

LIMK1 Pathway Mediated Alteration of Cofilin-1 Expression/Activity in CJD MM1 and VV2 Patients and in Pre-symptomatic and Symptomatic Stages of sCJD MM1 and VV2 Mice

This interaction of cofilin-1 with PrP^C suggests that there might be some functional correlation. So accordingly, we sought to explore molecular changes in cofilin-LIMK pathway in cerebellum and frontal cortex of two most frequent subtypes (MM1 and VV2) of sCJD, as well as age-matched controls (15 samples in each group). Total homogenates of the frontal cortex and cerebellum were analyzed using

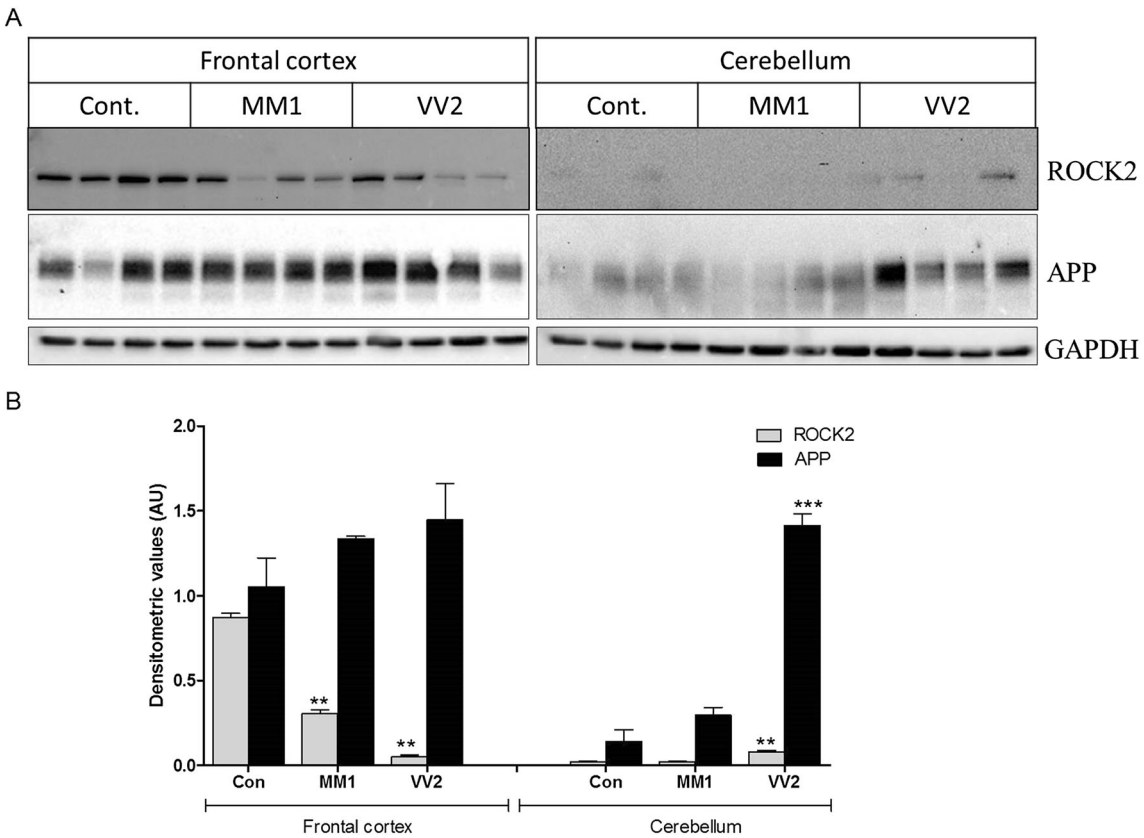

Fig. 5 Rock2 and APP in sCJD MM1 and VV2 subtypes. Western blotting analysis: **a** Rock2 and APP in four representative cases each for control, sCJD MM1, and sCJD VV2 cases; GAPDH immunostaining was used to normalize total protein loading. **b** Densitometry analysis from four independent (±SD) immunoblotting experiments of 15 control (Con), 15 MM1, and 15 VV2 cases. The significance was calculated with one-way ANOVA Friedman test (*$P < 0.05$, **$P < 0.01$, ***$P < 0.001$). *AU* arbitrary units

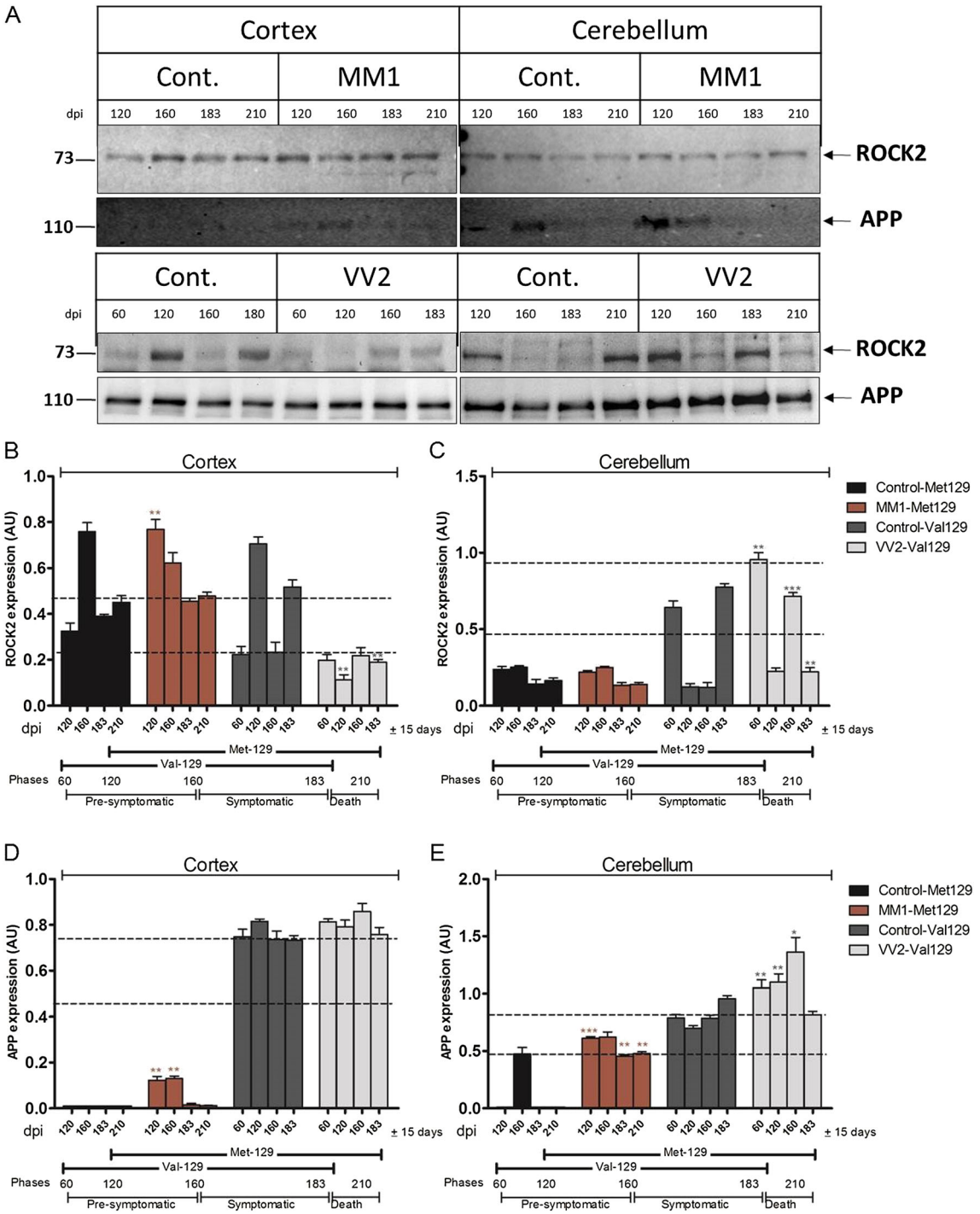

Fig. 6 Expression of Rock2 and APP at pre-symptomatic and symptomatic stage of sCJD MM1 and VV2 in mice. Tg340 mice expressing about 4-fold level of human PrPM129 were infected with sCJD MM1 and also VV2 10% brain homogenates. Samples were collected at indicated days post-infection (dpi): pre-symptomatic stage (60 dpi in VV2, 120 dpi in MM1) and symptomatic stages (120–183 dpi in VV2 and 160–210 dpi). **a** Rock2 and APP expressions in the cortex and cerebellum were observed by Western blot analysis using Rock2 and APP antibodies. **b**–**e** Densitometry analysis from four independent (±SD) immunoblotting experiments of Rock2 and APP from control and sCJD MM1- and VV2-infected PrPM129 mice in cortex and cerebellum. The significance was calculated with one-way ANOVA Friedman test (*$P < 0.05$, **$P < 0.01$, ***$P < 0.001$)

cofilin-1 and p-cofilin(Ser3) monoclonal antibodies (Fig. 2). Densitometry analysis revealed significantly altered cofilin-1 expression at the protein level in the frontal cortex in the sCJD MM1 subtype (Fig. 2c) and in the cerebellum of VV2 subtype as compared to age-matched control subjects (Fig. 2a, c), showing that the response was region-

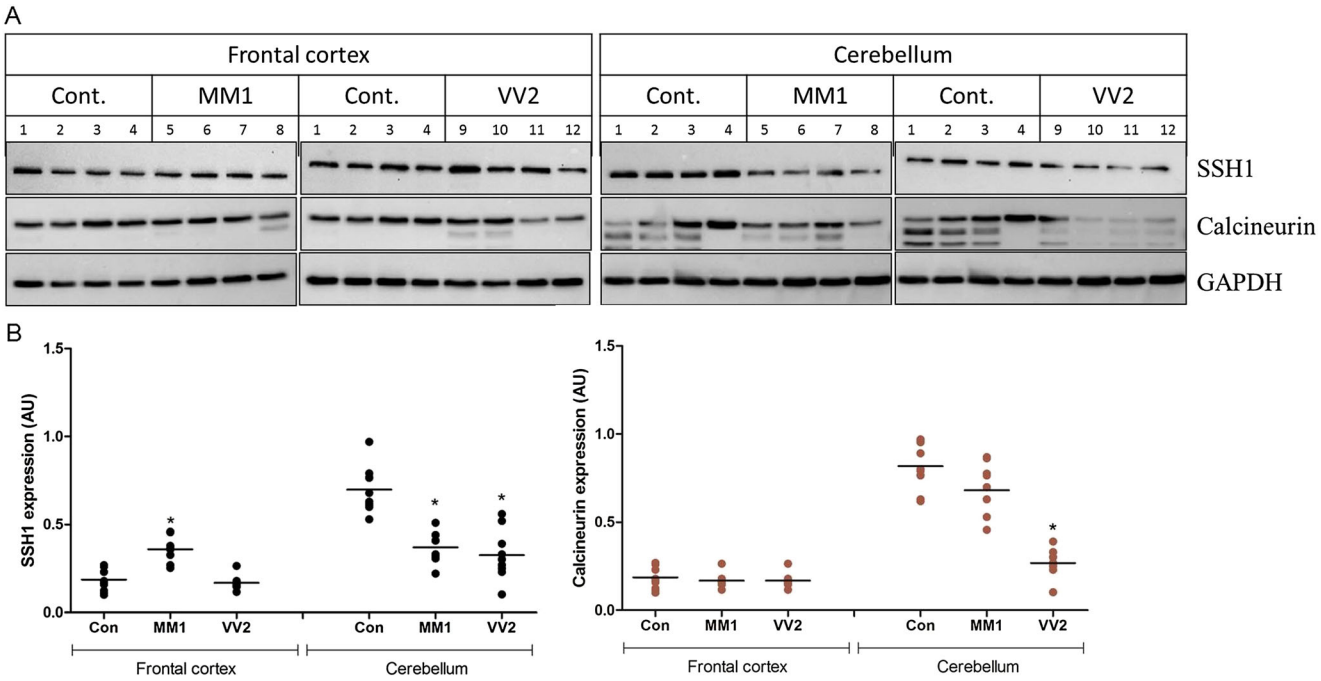

Fig. 7 SSH1 and calcineurin in sCJD MM1 and VV2 subtypes. Western blotting analysis: **a** SSH1 and calcineurin in four representative cases each for control, sCJD MM1, and sCJD VV2 cases; GAPDH immunostaining was used to normalize total protein loading. **b**, **c** Densitometry analysis from four independent (±SD) immunoblotting experiments of 15 control (Con), 15 MM1, and 15 VV2 cases. The significance was calculated with one-way ANOVA Friedman test (*$P < 0.05$). Region-dependent significantly altered expression is found in both sCJD subtypes compared to controls. *AU* arbitrary units

and codon 129 polymorphism-specific. Interestingly, for the phosphorylated form of cofilin-1, there was significant upregulation in levels of p-cofilin(Ser3) in frontal cortex and cerebellum region of MM1 subtype and in frontal cortex of VV2 subtype (Fig. 2a, d). This increased phosphorylation of cofilin-1 suggests that there is an inactivation of cofilin-1 in diseased brain. As cofilin is phosphorylated by LIM-kinase (LIMK) family of protein kinases including LIMK1 and LIMK2 (which inhibit activity of cofilin by phosphorylation) [48]; LIMKs are activated through phosphorylation at Thr505 and Thr508. We measured a significant decrease in total LIMK1 protein levels in cerebellum and frontal cortex of MM1 subtype vs. control and also in cerebellum of VV2 subtype (Fig. 2b, e). In contrast, the level of phosphorylated LIMK1 was significantly upregulated in the frontal cortex MM1 subtype and in cerebellum VV2 subtype as compared to age-matched control (Fig. 2a, f). As LIMK1 is regulated upstream by Rock2 and APP, we further demonstrated alterations in Rock2 and APP protein levels in frontal cortex and in cerebellum of MM1 and VV2 subtype (Fig. 5).

Time course study in sCJD MM1-inoculated Tg340 mice showed significant decrease in levels of cofilin-1 protein at pre-symptomatic and symptomatic stage of the disease (from 120 to 210 dpi) in cortex region of Met129 mice. In contrast, cofilin-1 levels were significantly increased in the cerebellum region at pre-symptomatic and symptomatic stage of the disease (from 120 to 210 dpi) (Fig. 3a, b). The p-cofilin(Ser3) levels showed upregulation in the cortex region of MM1-M129 mice as compared to VV2-Val129 mice (Fig. 3a, c–e). The cerebellum region of MM1-Met129 subtype sCJD showed a significant decrease of p-cofilin(Ser3) at pre-symptomatic stage (120 dpi) and upregulation at symptomatic stage (210 dpi) (Fig. 3d, f). In parallel, the cerebellum VV2-Val129 subtype showed increase of p-cofilin(Ser3) only at pre-symptomatic stages (120 dpi) (Fig. 3a, f).

This early stage regulated response of phosphorylation (deactivation) of cofilin indicating that cofilin activity decreases at the pre-symptomatic stage of the disease, and to explore the mechanism of this altered activity of cofilin-1, we analyzed changes in LIMK1, the modulator of cofilin phosphorylation. The MM1-Met129 mice showed significant decrease of LIMK1 at pre-symptomatic stage of the disease (from 120 to 160 dpi) in cortex region of MM1-Met129 mice cortex (Fig. 4a, b); however, P-LIMK1 showed significant increase at pre-symptomatic stage of the disease (120 dpi) in cortex region of MM1-Met129 mice (Fig. 4d, e). MM1-Met129 mice cerebellum showed upregulation of LIMK1 at pre-symptomatic stage of the disease (120 dpi) (Fig. 4a, c), and P-LIMK1 showed significant decrease at pre-symptomatic stage of the disease (120 dpi) (Fig. 4d, f). VV2-Val129 mice cerebellum showed upregulation of LIMK1 and P-LIMK1 at pre-symptomatic stage of the disease (160 dpi) (Fig. 4a, c, f).

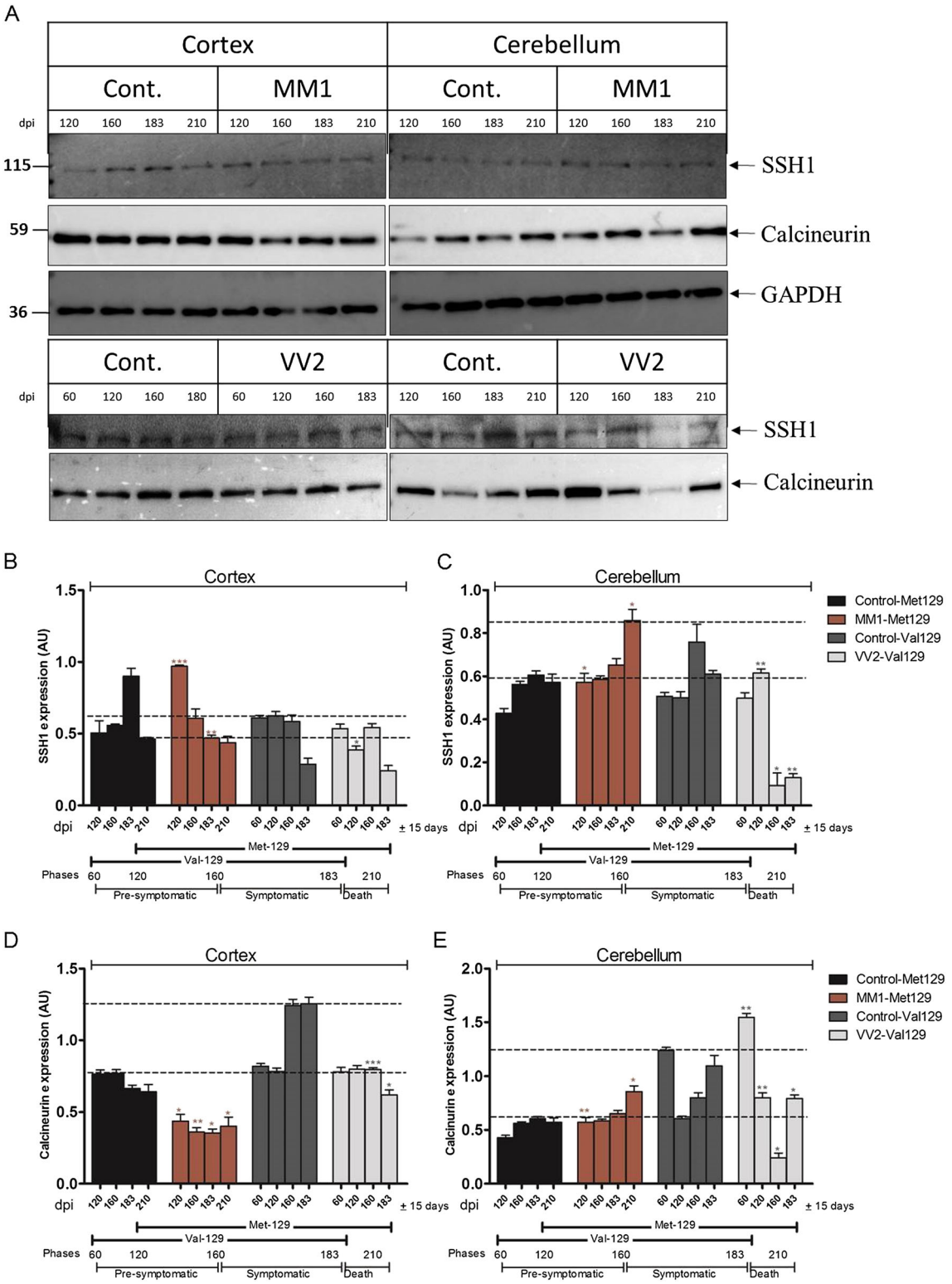

Fig. 8 Expression of SSH1 and calcineurin at pre-symptomatic and symptomatic stage of sCJD MM1 and VV2 in mice. Tg340 mice expressing about 4-fold level of human PrPM129 were infected with sCJD MM1 and also VV2 10% brain homogenates. Samples were collected at indicated days post-infection (dpi): pre-symptomatic stage (60 dpi in VV2, 120 dpi in MM1) and symptomatic stages (120–183 dpi in VV2 and 160–210 dpi). **a** SSH1 and calcineurin expression in the cortex and cerebellum were observed by Western blot analysis using SSH1 and calcineurin antibodies. **b**–**e** Densitometry analysis from four independent (±SD) immunoblotting experiments of SSH1 and calcineurin from control and sCJD MM1- and VV2-infected PrPM129 mice in cortex and cerebellum. The significance was calculated with one-way ANOVA Friedman test (*$P < 0.05$, **$P < 0.01$, ***$P < 0.001$)

Lastly, to demonstrate the kinases that regulate phosphorylation of LIMK, we found significant upregulation of Rock2 and APP at pre-symptomatic stage of the disease in MM1-Met129 and VV2-Val129 Tg340 mice (Figs. 5 and 6).

SSH1 and Calcineurin Altered Expression in sCJD MM1 and VV2 Subtypes and in Pre-symptomatic and Symptomatic Stages of sCJD MM1 Mice

Further, to better understand the aberrant cofilin-1 expression/activity, we analyzed changes in cofilin phosphatase SSH1 and its upstream regulator calcineurin by Western blot in frontal cortex and cerebellum samples from sCJD cases with the subtypes MM1 and VV2, as well as age-matched controls. Total homogenates of the frontal cortex and cerebellum were analyzed using SSH1 and calcineurin monoclonal antibodies (Fig. 7a). Remarkably, in the cerebellum, SSH1 expression was significantly decreased in both subtypes MM1 and VV2 as compared to age-matched control samples (Fig. 7a, b) while SSH1 levels were increased in frontal cortex of MM1 subtype. However, calcineurin expression was significantly decreased only in VV2 subtype in the cerebellum (Fig. 7a, c) showing that the response was region-specific and codon 129 polymorphism-specific. Furthermore, sCJD MM1-inoculated mice demonstrated a significant increase in the expression of SSH1 at the pre-symptomatic stage (120 dpi), in contrary to sCJD VV2-inoculated mice showing significant decrease at pre-symptomatic stage (60 and 120 dpi) in the cortex (Fig. 8a, b). However, sCJD MM1-inoculated mice demonstrated a significant decrease in the expression of SSH1 at the symptomatic stage (183 dpi) in the cortex. The terminal or death stage showed no significant regulation in both subtypes of sCJD MM1- and VV2-inoculated mice (Fig. 8a, b). The cerebellum region of both subtypes of sCJD-inoculated mice showed differential regulation of SSH1 (Fig. 8a, c). The expression of calcineurin showed significant decrease in the cortex of sCJD MM1 mice at pre-symptomatic and symptomatic stages (from 120 to 210 dpi terminal stage). In contrast, in the sCJD VV2-inoculated mice, the calcineurin expression was significantly downregulated only in symptomatic stages (from 160 to 183 dpi terminal stage) (Fig. 8a, d). In cerebellum, calcineurin expression in sCJD MM1-inoculated mice showed a significant increased expression in the pre-symptomatic stage and symptomatic terminal stages (120 and 210 dpi terminal stage) (Fig. 8a, e). The sCJD VV2-inoculated mice in the cerebellum showed a significant upregulation of calcineurin in the pre-symptomatic stages (60 and 120 dpi) (Fig. 8a, e). However, symptomatic and terminal death stages showed downregulation (160 and 183 dpi) (Fig. 8a, e).

siRNA-Induced Gene Silencing of Cofilin-1 Leads to Dense Accumulation of F-Actin, Activation of Microglia, and Decreased Cell Viability

To check the cofilin-1-dependent actin depolymerization activity, we demonstrated that cofilin-1 siRNA knockdown lead to increased expression level of F-actin and decreased expression level of PrP^C. Approximately 70–80% of cofilin-1 expression depletion was achieved in PCNs (Fig. 9a, c). The immunofluorescence results demonstrated that cofilin-1 siRNA deficit cells showed increased expression level and dense accumulation of F-actin (Fig. 9a, b). However, PrP^C showed decreased expression and altered localization pattern (Fig. 9a, d). The percent colocalization of cofilin-1 and F-actin showed significant decrease in the cofilin-1 depleted PCNs. However, F-actin and PrP^C showed significant upregulation of percent colocalization in the cofilin-1 depleted PCNs (Fig. 9e, f).

As cofilin-1 gene deletion leads to lethality in mouse [49], further, we investigated the effect of cofilin-1 depletion on cell viability in both PrP^C wild-type and knockout PCN cells. Cofilin-1 depletion resulted in decreased Cell viability in both PrP^C wild-type and knockout PCN cells (Fig. 10a) while concomitantly increased caspase-3 activity (Fig. 10b). Interestingly, PrP^C-expressing PCNs with siRNA cofilin-1 depletion, showed more viability and less caspase-3 activation as compared to $PrP^{-/-}$ PCNs depleted with cofilin-1 (Fig. 10a, b); suggesting protective role of PrP^C on cell viability.

As both in vitro and in vivo studies have shown that neuronal apoptosis and neuronal death precedes microglia activation [50], so accordingly, we investigated the activation status of microglia in cofilin-1 depleted PCN cultures (PrP^C wild-type and PrP^C knockout cells). Here, we demonstrated a correlation between presence and absence of PrP^C, and the cofilin-1 depletion induced microglial activation in primary cortical neurons (Fig. 10c–e). Immunofluorescence data demonstrated the different populations of microglia after siRNA against cofilin-1 treatment in PCNs (Fig. 10c) with a shift towards activated microglia in cofilin-1 depleted cells. These microglia populations showed marked differences in the expression of cofilin-1 and p-cofilin with the upregulation of p-cofilin in activated microglia (Fig. 11a). The colocalization analysis of cofilin-1, and p-cofilin(Ser3) with Iba1 showed significant increase shift between p-cofilin and Iba1 in the cofilin-1-depleted PCNs as compared to control (Fig. 11b, c). Overall, coflin-1 regional density, distribution, and/or activity of microglia and microglia-derived factors may influence the region-specific role for this cell type (Fig. 13).

Further, it is already been reported that the microglia showed upregulation in sCJD cases, with increased expression levels in the frontal cortex in MM1 and in the cerebellum in

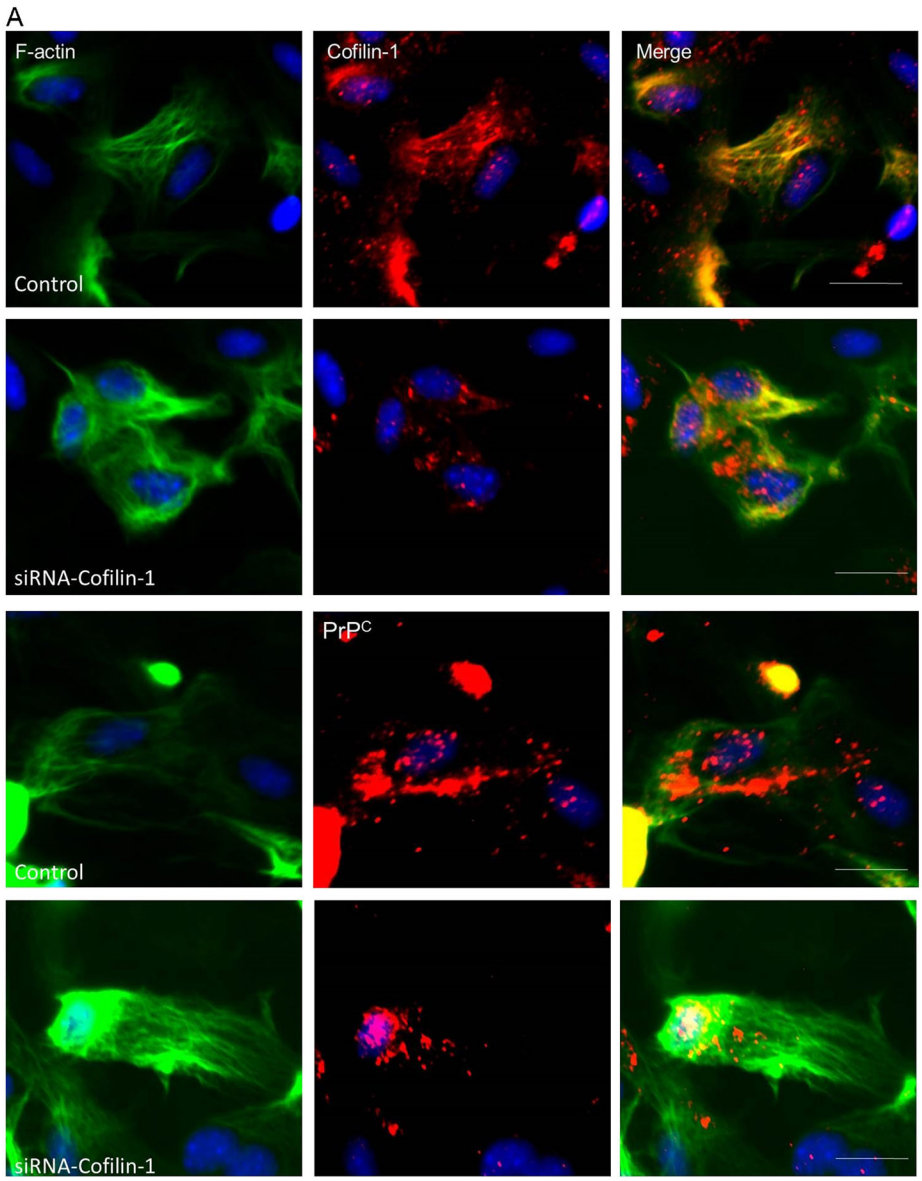

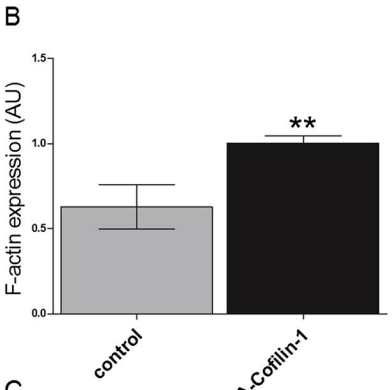

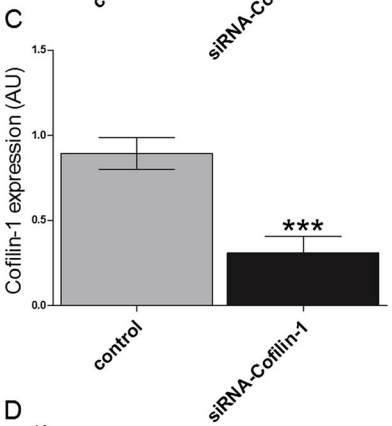

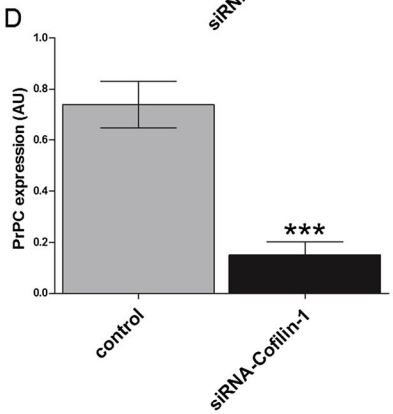

E

Nr.	Rr	Coloc. Coefficient F-actin (M1)	Coloc. Coefficient Cofilin-1 (M2)	% Colocalization
Control	0.374	0.789	0.849	2.18
siRNA-Cofilin-1	0.425	0.998	0.989	0.91
			Coloc. Coefficient PrPC(M2)	
Control				3.01
siRNA-Cofilin-1	0.735			4.91

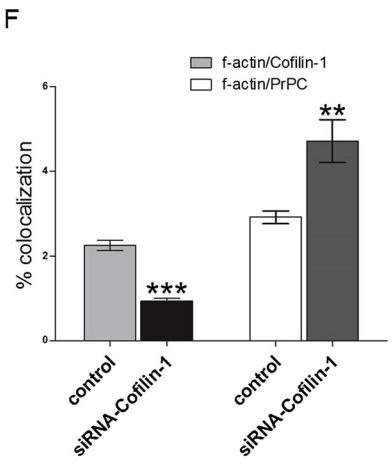

VV2 cases. In the CJD MM1 mice, the microglial marker Iba1 also showed upregulation at mRNA level [51]. Our data also showed region-specific upregulation of iba1 levels, microglia marker, in sCJD cases for both subtypes MM1 and VV2

◀ **Fig. 9** Colocalization of F-actin, cofilin-1, and PrP^C in PCNs after depletion of cofilin-1. Primary cultures of mouse cortex neurons (PCNs) were prepared from pregnant mice at embryonic day 14; the mice were *prnp* (the PrP-encoding gene). PCNs were treated with cofilin-1 siRNA and fixed and immunostained for F-actin, cofilin-1, and PrP^C examples from a single neuron showing **a** co-immunostaining of F-actin and cofilin-1, F-actin, and PrP^C. **b**, **c**, **d** Quantification of images taken in different regions of neurons fixed after siRNA depletion and showed a significant (**$P < 0.01$) increase in F-actin expression and a decrease of cofilin-1 expression (***$P < 0.001$) and PrP^C (***$P < 0.001$). **e**, **f** Pearson's colocalization correlation coefficient rp ($-1 \leq rp \leq 1$) experiments and graph was generated by ImageJ (WCIF plugin) software. Quantification of colocalization was determined with and without cofilin-1 siRNA treatment by ImageJ (WCIF plugin) software. Densitometry analysis from four independent (±SD) experiments and significance was calculated with Student's *t* test (**$P < 0.01$, ***$P < 0.001$)

(Fig. 12). We also found significant upregulation of iba1 expression at pre-symptomatic stage and symptomatic stage of the disease in MM1-Met129 and VV2-Val129 Tg340 mice (Fig. 12).

Discussion

Selective Interactive Association Between PrP^C and Cofilin-1

We have previously shown that by using interactomic approaches, we can isolate cofilin-1 as a binding partner of PrP^C in HpL3–4 cells [46]; however, the prion-specific regulatory response of cofilin-1 and its activation during prion disease progression remained to be determined. In this study, we showed that the cofilin-1 and phosphorylated form of cofilin at Ser3 interacts and co-sediment with PrP^C in primary cortical and cerebellar neurons. Cofilin-1, which is a member of cofilin-actin cytoskeleton assembly and is involved in abnormal rod formation [52], specifically in cortical region of AD brain [52], has shown direct interaction with PrP^C in our study, suggesting a role of cofilin-1 in pathogenesis of Prion diseases. Previously, cofilin-1 has been shown as an interactive partner of PrP^{Sc} [47], further supporting the notion that there might be some functional association between cofilin-1 and prion protein. Altogether, our results indicate that there is a functional correlation between PrP^C, PrP^{Sc}, and cofilin-1 in relation to strain-specific prion diseases and with disease progression rate.

Cofilin-Phosphorylation/Dephosphorylation Pathway in sCJD MM1 and VV2 Subtypes: Early and Terminal Stage Disease Progression Association

In different cellular processes, actin is modulated by cofilin [26], and it has been hard to demonstrate that if the cofilin rod formation has damaging effects on cells, or whether it is the modification of cofilin pathway at some other step. To uncover this condition, we have taken an approach to check the alteration in cofilin-1 upstream pathway at symptomatic stage (in humans and mice) and pre-symptomatic stage (in mice) of the disease (Fig. 13).

In our regional and temporal studies, cofilin-1 (de-phosphorylated/active form) expression at protein level was significantly altered in the frontal cortex in the sCJD MM1 subtype. Interestingly, cofilin-1 (de-phosphorylated/active form) levels were significantly decreased in the cerebellum in VV2 subtype only. Levels of phosphorylated (de-activated) form which is unable to bind to actin were significantly increased in the frontal cortex in CJD-MM1 and in the cerebellum and frontal cortex of CJD-VV2 patients, suggesting that there is an increase in the inactivated form (phosphorylated form) of cofilin-1 in diseased brain. In the case of AD, cofilin overactivation and rod formation is well known [53, 54]; in contrast, we observed cofilin inactivation (increased phosphorylation) particularly at terminal stage of the disease in CJD patients, which suggest that response is CJD-specific. The novelty of our work is to report for the first time changes in cofilin pathway in CJD, thus indicating an involvement of cofilin in lesion development in prion diseases.

Time course study in sCJD MM1 and VV2-inoculated Tg340 mice showed a significant increase of p-cofilin(Ser3) in the cortex region at pre-symptomatic and symptomatic stage of the disease (from 120 to 210 dpi). In parallel, the cerebellum VV2 subtype showed increase of p-cofilin(Ser3) only at pre-clinical stages (120 dpi). LIMK1; phosphorylation activator of cofilin-1 at Ser3 showed significant altered regulatory response corresponding to the cofilin phosphorylation state in cortex and cerebellum and in both MM1 and VV2 subtype-inoculated Tg340 mice.

This early stage regulated response of phosphorylation (de-activation) of cofilin-1 indicates that cofilin-1 activity decreases at the pre-symptomatic stage of the disease. LIMK1 is responsible for the phosphorylation of cofilin and is activated by phosphorylation at thr505 and th508, which showed a 2-fold increase in the phosphorylation level of kinase, which indicates a stronger LIMK activity as early disease response. Finally, among the kinases that phosphorylate LIMK is RhoA-associated kinase (Rock2) whose activity is regulated by small G protein RhoA [27–29] and amyloid precursor protein (APP). Initially, there was an increase in Rock2 levels at 60 dpi, which return to normal at 120 dpi, and then increase again at 180 dpi, probably associated with different pattern of PrP^{Sc} aggregates in these mice. We previously reported that the RhoA activity was regulated by phosphorylation of myosin light-chain (MLC) in association with Arf1-dependent PI3K pathway [36]. The APP showed significant upregulation at pre-symptomatic stage of the disease in MM1- and VV2-inoculated Tg340 mice. These data argue that the phosphorylation (de-activation) of cofilin at Ser3 is regulated by the upstream activation of the RhoA-Rock2-LIMK1-pathway at early stage of the disease.

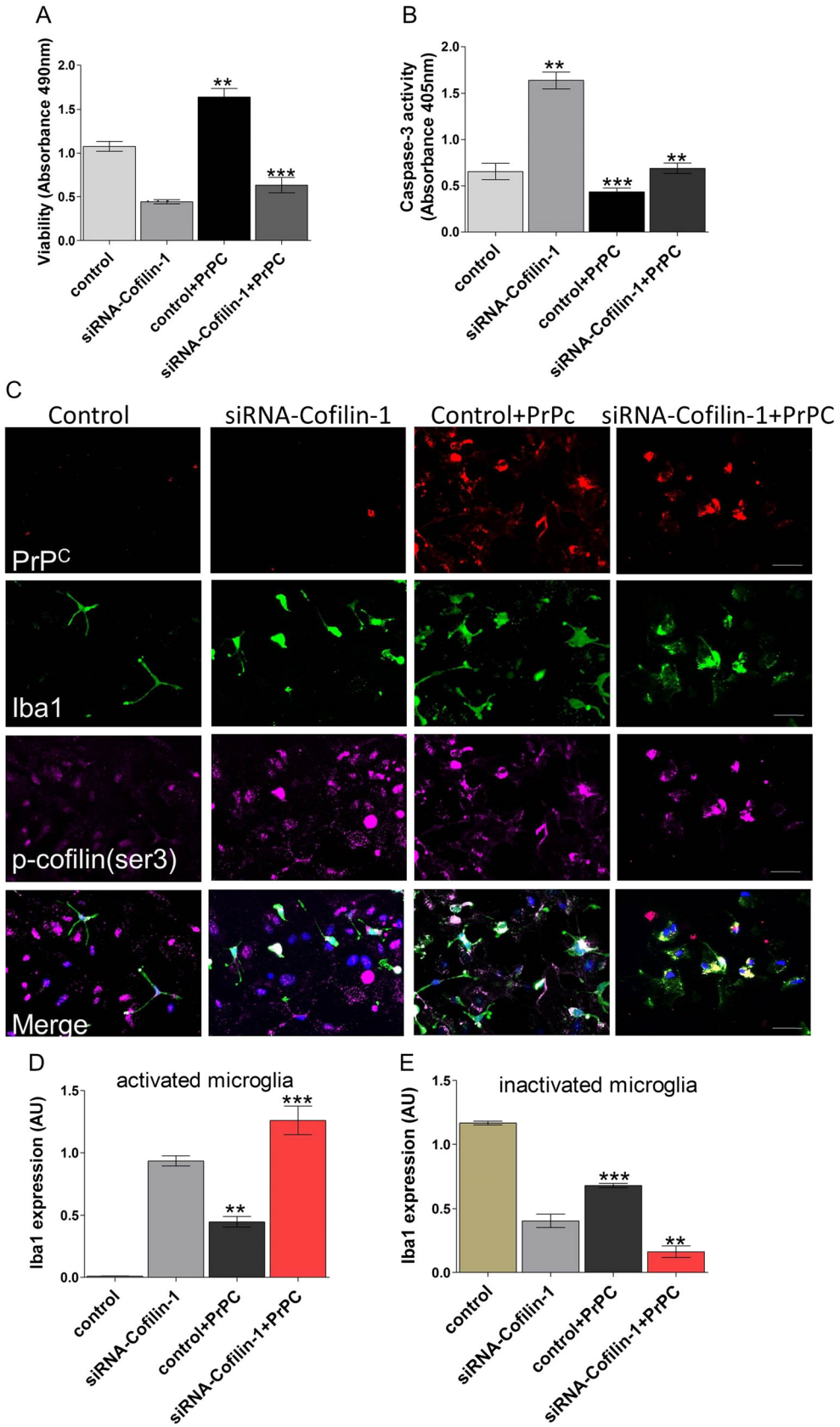

The reactivation of cofilin-1 by dephosphorylation at Ser3 is SSH1 dependent in neurons [55]. However, pathways for p21-LIM kinase activation, protein kinase C/G, or reactive oxygen species were not responsible for these alterations

◀ **Fig. 10** PCN viability and activation of microglia after depletion of cofilin-1. Primary cultures of mouse cortex neurons (PCNs) were prepared from pregnant mice at embryonic day 14; the mice were *prnp* (the PrP-encoding gene). PCNs were treated with cofilin-1 siRNA. **a** Cell viability was measured by MTS assay 48 h post transfection. The viability values are shown as absorbance at 490 nm. Data points are the means ± SEM of values from four different experiments. The cells expressing PrP^C displayed elevated level of cell viability under cofilin-1 depletion as compared with out PrP^C. The significance was performed by one-way ANOVA Friedman test (**$P < 0.01$, ***$P < 0.001$). **b** Caspase-3 activity was detected by fluorescence measurement of the cleaved pNA from the substrate peptide DEVD-pNA. Data points are the means ± SD of values from four different experiments. The cells expressing PrP^C displayed decreased level of caspase-3 cleavage activity under cofilin-1 depletion as compared with out PrP^C. The significance was performed by one-way ANOVA Friedman test (**$P < 0.01$, ***$P < 0.001$). **c** Colocalization of PrP^C, Iba1, and p-cofilin(Ser3) in PCNs after depletion of cofilin-1, fixed and immunostained. **d**, **e** Quantification of images taken in different regions of neurons and showed a significant altered expression of activated and inactivated Iba1-positive microglia after siRNA depletion in the presence and absence of PrP^C expression. Quantification of colocalization was determined by ImageJ (WCIF plugin) software, and significance was calculated with Student's *t* test (**$P < 0.01$, ***$P < 0.001$)

regulation of LIMK1 [30].

To further explore the possible mechanism responsible for altered expression/activity of cofilin-1, we measured changes in cofilin phosphatase SSH1 and its upstream regulator calcineurin and found the altered response at early disease presymptomatic stage in both subtypes. Calcineurin is responsible for cofilin dephosphorylation either directly or indirectly via an intermediary phosphatase SSH1. Calcineurin has been implicated in the regulation of synaptic plasticity and memory [57, 58]. Hyperactivation of calcineurin leads to synaptic abnormalities and neuronal death [59]. On the other side, SSH1 also deactivates LIMK1 to regulate cofilin activation state and could be the risk factor for the modulation of the whole pathway. The mechanism responsible for cofilin-1 activation or inactivation/

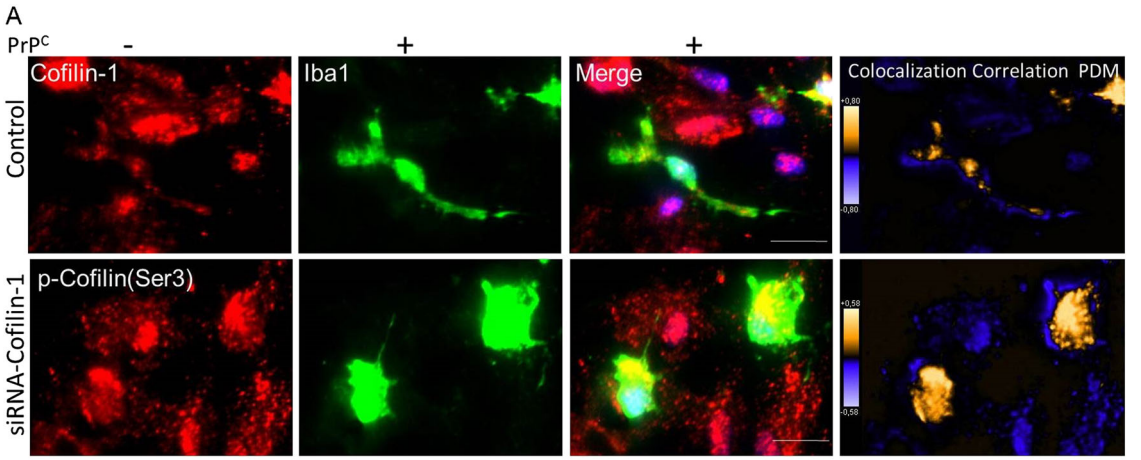

B

Nr.	Rp	Coloc. Coefficient p-cofilin-1 (M1)	Coloc. Coefficient Iba1 (M2)	% Colocalization
1.	0.247	0.789	0.849	0.48
2.	0.425	0.998	0.989	3.78

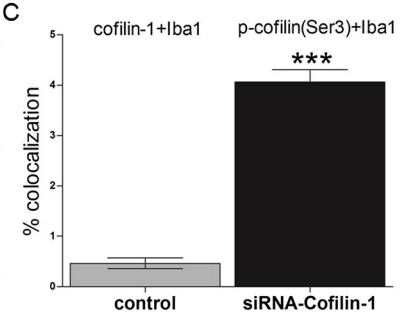

Fig. 11 Colocalization of cofilin-1 and p-cofilin(Ser3) in PCNs after depletion of cofilin-1. Primary cultures of mouse cortex neurons (PCNs) were prepared from pregnant mice at embryonic day 14; the mice were *prnp* (the PrP-encoding gene). PCNs were treated with cofilin-1 siRNA and fixed and **a** co-immunostained for cofilin-1 and p-cofilin(Ser3). **b**, **c** Quantification of images taken in different regions of neurons fixed after siRNA depletion and showed a significant redistribution of p-cofilin(Ser3) in activated form of Iba1-positive microglia. Pearson's colocalization correlation coefficient rp ($-1 \le rp \le 1$) experiments and graph were generated by ImageJ (WCIF plugin) software. Quantification of colocalization that was determined with and without cofilin-1 siRNA treatment showed significant increase of p-cofilin(Ser3) in Iba1-positive microglia. Densitometry analysis from four independent (±SD) and significance was calculated with Student's *t* test (***$P < 0.001$)

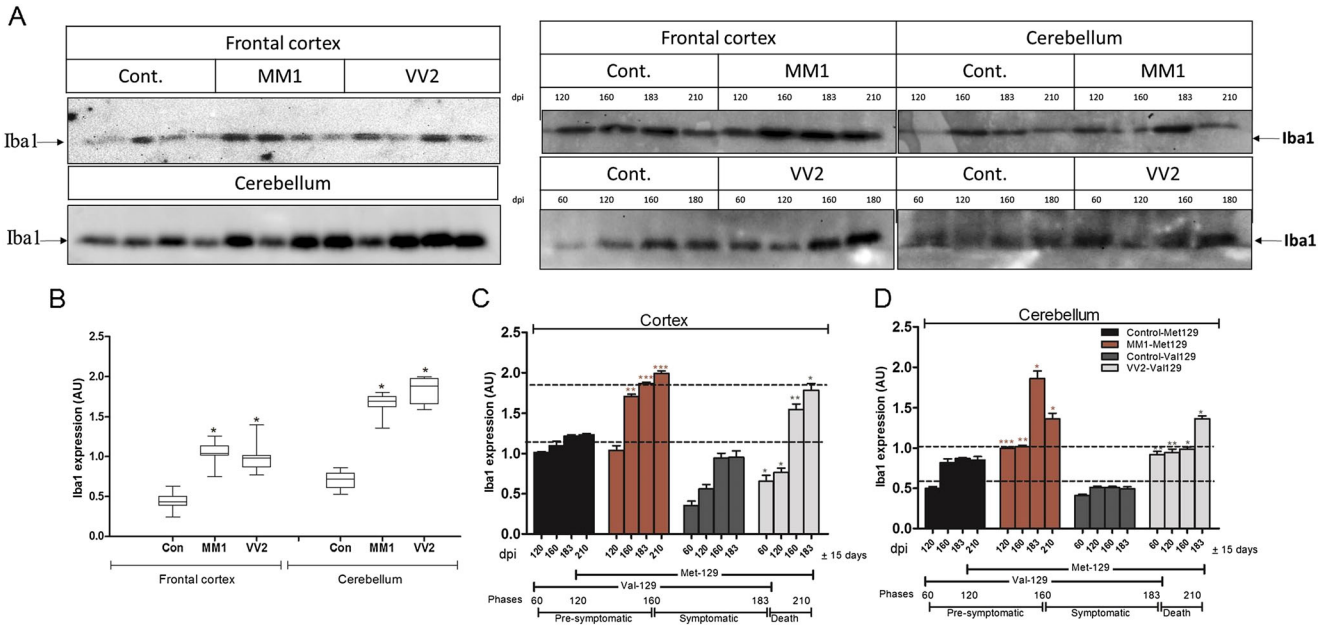

Fig. 12 Iba1 expression in sCJD MM1 and VV2 subjects and at pre-symptomatic and symptomatic stage of sCJD MM1 and VV2 mice. Western blotting analysis: **a** Iba1 protein expression in four representative cases each for control, sCJD MM1, and sCJD VV2 cases and in Tg340 mice infected with sCJD MM1 and also VV2 10% brain homogenates. Samples were collected at indicated days post-infection (dpi): pre-symptomatic stage (60 dpi in VV2 120 dpi in MM1) and symptomatic stages (120–183 dpi in VV2 and 160–210 dpi). **b** Densitometry analysis from four independent (±SD) immunoblotting experiments of 15 control (Con), 15 MM1, and 15 VV2 cases. **c**, **d** Densitometry analysis from four independent (±SD) immunoblotting experiments Iba1 from control and sCJD MM1- and VV2-infected PrPM129 mice in cortex and cerebellum. The significance was calculated with one-way ANOVA Friedman test (*$P < 0.05$). Region-dependent significantly altered expression is found in both sCJD subtypes compared to controls. *AU* arbitrary units

phosphorylation may be different in both subtypes and brain regions and dependent, at least in part, on PrP^{Sc} aggregates.

Dense Accumulation of F-Actin and Activation of Microglia

The activation of cofilin-1 (dephosphorylation) is a key factor for the dynamics in actin depolymerization and cytoskeleton assembly [60]. Cofilin phosphorylation was aberrantly upregulated in the terminal stage of the disease, in parallel to the reduction of the SSH1. Interestingly, our findings indicate that cofilin-1 depletion leads to denser actin filaments corresponding to repression of level of PrP^{C} in PCNs. The reason for decreased levels of PrP^{C} might be altered actin dynamics leading to proteasome degradation of PrP^{C} instead of its transportation to the cell membrane due to lack of cofilin-1-dependent remodeling of actin cytoskeleton [61] as the localization pattern of PrP^{C} was also altered in cofilin-1 depleted cells. Several recent studies also support the idea that alterations in cofilin activation state contribute to actin pathology in neurodegeneration.

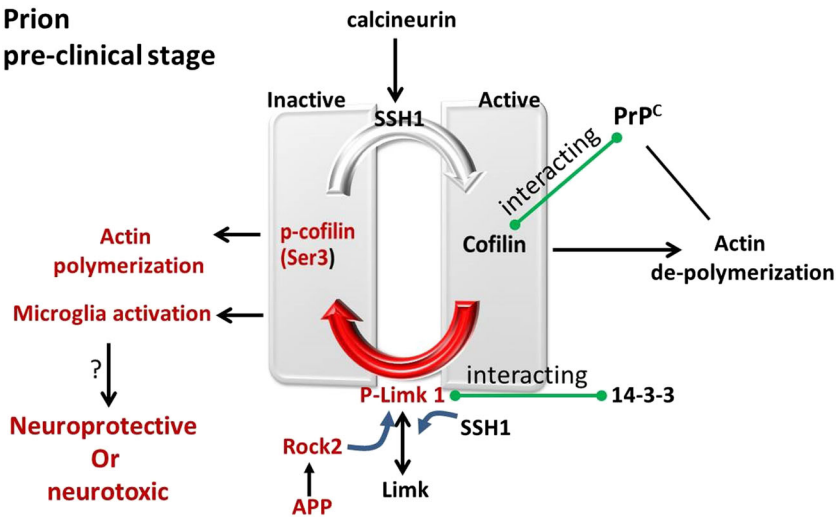

Fig. 13 Schematic representation of molecular events of cofilin-LIMK-SSH1-dependent actin assembly showed altered response at pre-symptomatic stage and symptomatic stage of the disease. *Yellow* highlighted area presents alterations demonstrated in this study (color figure online)

The activation of microglial is a trademark of the neuroimmunological response in prion disease [62]. Recent report demonstrated the suggestive role of microglia during the clearance of cofilin aggregation [53]. Our data demonstrated different populations of microglia in response to depletion of cofilin-1 and presence of PrP^C. The different activation statuses of microglia after depletion of cofilin-1 demonstrate a link between cofilin-1, PrP^C, and microglia activation during the course of prion disease. These different microglia populations showed marked differences in the expression of dephosphorylated form (active form) in non-active microglia and phosphorylated form (inactivated) of cofilin in activated form of microglia.

However, the upregulated microglia expression showed disease subtype and brain region-specific response in CJD patients (Fig. 12). CJD-MM1 patients showed significantly and specifically upregulated microglia in frontal cortex; however, CJD-VV2 subtype patients showed this response specifically in cerebellum [51].

Altogether, our data demonstrated the different populations of microglia in response to depletion of cofilin-1, presence of PrP^C, and disease subtype manner. These microglia populations showed marked differences in the expression of dephosphorylated form of cofilin in non-active microglia and phosphorylated form of cofilin in activated microglia. Cofilin-1 regional density, distribution, and/or activity of microglia and microglia-derived factors may influence the region-specific role for this cell type.

This regional and subtype-specific post-translational altered pattern of cofilin-LIMK-APP pathway in sCJD MM1 and VV2 and a modified temporal response in sCJD MM1 and VV2 mice could correlate with the disease severity and progression in neurons in correlation with microglia. The demonstration in respect with subtype manner could prove to be the cardinal specific targets for therapeutic intervention.

Conclusion

In conclusion, this study demonstrates altered cofilin-LIMK-SSH1 pathway in sporadic CJD-MM1 and VV2 subtypes at early disease stage in a strain-specific subtype manner. The regulated response may contribute actin cytoskeleton abnormalities that ultimately lead to synapse and dendritic spine loss, as actin dynamics are responsible for synapse formation, maturation, and stability and for maintenance of dendritic spines in CJD. Taken together, our findings highlight a key pre-and early symptomatic role of cofilin-1 activation in neurodegeneration specifically as an early regulatory response, suggesting the idea that targeting the cofilin signaling axis might be a promising strategy and a potential early diagnostic approach useful to reveal therapeutic strategy for misfolded protein differential response.

Acknowledgements We give special thanks to Dr. Torres at CISA INIA who produced the tg340 mice.

Compliance with Ethical Standards Human samples from the Institute of Neuropathology Brain Bank (HUB-ICO-IDIBELL Biobank) and Biobank of Hospital Clinic-IDIBAPS were obtained following the Spanish legislation (Ley de la Investigación Biomédica 2013 and Real DecretoBiobancos 2014) and the approval of the local ethics committees.

All animal experiments were performed in accordance with the ethical standard set by Regierungspräsidium Tübingen (Regional Council) Experimental No. FLI 231/07 file reference number 35/9185.81-2. All animal experiments have been performed in compliance with the institutional and French national guidelines, in accordance with the European Community Council Directive 86/609/EEC. The experimental protocol was approved by the INRA Toulouse/ENVT ethics committee.

References

1. Tschampa HJ, Kallenberg K, Kretzschmar HA, Meissner B, Knauth M, Urbach H, Zerr I (2007) Pattern of cortical changes in sporadic Creutzfeldt-Jakob disease. Am J Neuroradiol 28:1114–1118
2. Bishop MT, Will RG, Manson JC (2010) Defining sporadic Creutzfeldt-Jakob disease strains and their transmission properties. Proc Natl Acad Sci 107:12005–12010
3. Parchi P, Giese A, Capellari S, Brown P, Schulz-Schaeffer W, Windl O, Zerr I, Budka H et al (1999) Classification of sporadic Creutzfeldt-Jakob disease based on molecular and phenotypic analysis of 300 subjects. Ann Neurol 46:224–233
4. Parchi P, Strammiello R, Notari S, Giese A, Langeveld JP, Ladogana A, Zerr I, Roncaroli F et al (2009) Incidence and spectrum of sporadic Creutzfeldt-Jakob disease variants with mixed phenotype and co-occurrence of PrPSc types: an updated classification. Acta Neuropathol 118:659–671
5. Ferrer I, Puig B, Blanco R, Marti E (2000) Prion protein deposition and abnormal synaptic protein expression in the cerebellum in Creutzfeldt-Jakob disease. Neuroscience 97:715–726
6. Jeffrey M, Halliday WG, Bell J, Johnston AR, Mac Leod NK, Ingham C, Sayers AR, Brown DA et al (2000) Synapse loss associated with abnormal PrP precedes neuronal degeneration in the scrapie-infected murine hippocampus. Neuropathol Appl Neurobiol 26:41–54
7. Jeffrey M, McGovern G, Sisó S, González L (2011) Cellular and sub-cellular pathology of animal prion diseases: relationship between morphological changes, accumulation of abnormal prion protein and clinical disease. Acta Neuropathol 121:113–134
8. Loubet D, Dakowski C, Pietri M, Pradines E, Bernard S, Callebert J, Ardila-Osorio H, Mouillet-Richard S et al (2012) Neuritogenesis: the prion protein controls beta1 integrin signaling activity. FASEB J 26:678–690
9. Zafar S, Younas N, Correia S, Shafiq M, Tahir W, Schmitz M, Ferrer I, Andreoletti O et al (2016) Strain-specific altered regulatory response of Rab7a and Tau in Creutzfeldt-Jakob disease and Alzheimer's disease. Mol Neurobiol
10. Eiseler T, Hausser A, De Kimpe L, Van Lint J, Pfizenmaier K (2010) Protein kinase D controls actin polymerization and cell motility through phosphorylation of cortactin. J Biol Chem 285: 18672–18683
11. Munnamalai V, Weaver CJ, Weisheit CE, Venkatraman P, Agim ZS, Quinn MT, Suter DM (2014) Bidirectional interactions between NOX2-type NADPH oxidase and the F-actin cytoskeleton in neuronal growth cones. J Neurochemn/a
12. Yamada H, Abe T, Satoh A, Okazaki N, Tago S, Kobayashi K, Yoshida Y, Oda Y et al (2013) Stabilization of actin bundles by a

dynamin 1/cortactin ring complex is necessary for growth cone filopodia. J Neurosci 33:4514–4526
13. Bosch M, Castro J, Saneyoshi T, Matsuno H, Sur M, Hayashi Y (2014) Structural and molecular remodeling of dendritic spine substructures during long-term potentiation. Neuron Cell Press 82: 444–459
14. Okamoto K, Nagai T, Miyawaki A, Hayashi Y (2004) Rapid and persistent modulation of actin dynamics regulates postsynaptic reorganization underlying bidirectional plasticity. Nat Neurosci 7: 1104–1112
15. Schubert V, Dotti CG (2007) Transmitting on actin: synaptic control of dendritic architecture. J Cell Sci 120:205–212
16. Sekino Y, Kojima N, Shirao T (2007) Role of actin cytoskeleton in dendritic spine morphogenesis. Neurochem Int 51:92–104
17. Star EN, Kwiatkowski DJ, Murthy VN (2002) Rapid turnover of actin in dendritic spines and its regulation by activity. Nat Neurosci 5:239–246
18. Bravo-Cordero JJ, Magalhaes MA, Eddy RJ, Hodgson L, Condeelis J (2013) Functions of cofilin in cell locomotion and invasion. Nat Rev Mol Cell Biol 14:405–415
19. Hagedorn EJ, Kelley LC, Naegeli KM, Wang Z, Chi Q, Sherwood DR (2014) ADF/cofilin promotes invadopodial membrane recycling during cell invasion in vivo. J Cell Biol 204:1209–1218
20. Vitriol EA, Wise AL, Berginski ME, Bamburg JR, Zheng JQ (2013) Instantaneous inactivation of cofilin reveals its function of F-actin disassembly in lamellipodia. Mol Biol Cell 24:2238–2247
21. Kim T, Vidal GS, Djurisic M, William CM, Birnbaum ME, Garcia KC, Hyman BT, Shatz CJ (2013) Human LilrB2 is a beta-amyloid receptor and its murine homolog PirB regulates synaptic plasticity in an Alzheimer's model. Science 341:1399–1404
22. Bellenchi GC, Gurniak CB, Perlas E, Middei S, Ammassari-Teule M, Witke W (n.d.)
23. Goodson M, Rust MB, Witke W, Bannerman D, Mott R, Ponting CP, Flint J (2012) Cofilin-1: a modulator of anxiety in mice. PLoS Genet 8:e1002970
24. Gu J, Lee CW, Fan Y, Komlos D, Tang X, Sun C, Yu K, Hartzell HC et al (2010) ADF/cofilin-mediated actin dynamics regulate AMPA receptor trafficking during synaptic plasticity. Nat Neurosci 13:1208–1215
25. Rust MB, Gurniak CB, Renner M, Vara H, Morando L, Gorlich A, Sassoe-Pognetto M, Banchaabouchi MA et al (2010) Learning, AMPA receptor mobility and synaptic plasticity depend on n-cofilin-mediated actin dynamics. EMBO J 29:1889–1902
26. Van Troys M, Huyck L, Leyman S, Dhaese S, Vandekerkhove Jl, Ampe C (2008) Ins and outs of ADF/cofilin activity and regulation. Eur J Cell Biol
27. Gu H, Yu SP, Gutekunst CA, Gross RE, Wei L (2013) Inhibition of the Rho signaling pathway improves neurite outgrowth and neuronal differentiation of mouse neural stem cells. Int J Physiol Pathophysiol Pharmacol 5:11–20
28. Huang TY, Minamide LS, Bamburg JR, Bokoch GM (2008) Chronophin mediates an ATP-sensing mechanism for cofilin dephosphorylation and neuronal cofilin-actin rod formation. Dev Cell 15:691–703
29. Nishita M, Tomizawa C, Yamamoto M, Horita Y, Ohashi K, Mizuno K (2005) Spatial and temporal regulation of cofilin activity by LIM kinase and Slingshot is critical for directional cell migration. J Cell Biol 171:349–359
30. Mizuno K (2013) Signaling mechanisms and functional roles of cofilin phosphorylation and dephosphorylation. Cell Signal 25: 457–469
31. Kligys K, Yao J, Yu D, Jones JCR (2009) 14-3-3 zeta/tau heterodimers regulate Slingshot activity in migrating keratinocytes. Biochem Biophys Res Commun 383:450–454
32. Ladogana A, Sanchez-Juan P, Mitrova E, Green A, Cuadrado-Corrales N, Sanchez-Valle R, Koscova S, Aguzzi A et al (2009) Cerebrospinal fluid biomarkers in human genetic transmissible spongiform encephalopathiesa. J Neurol 256:1620–1628
33. Schmitz M, Ebert E, Stoeck K, Karch A, Collins S, Calero M, Sklaviadis T, Laplanche JL et al (2015) Validation of 14-3-3 protein as a marker in sporadic Creutzfeldt-Jakob disease diagnostic. Mol Neurobiol
34. Zerr I, Bodemer M, Weber T (1997) The 14-3-3 brain protein and transmissible spongiform encephalopathy. N Engl J Med 336:874–875
35. Llorens F, Ansoleaga B, Garcia-Esparcia P, Zafar S, Grau-Rivera O, Lopez-Gonzalez I, Blanco R, Carmona M et al (2013) PrP mRNA and protein expression in brain and PrP(c) in CSF in Creutzfeldt-Jakob disease MM1 and VV2. Prion 7:383–393
36. Zafar S, Schmitz M, Younus N, Tahir W, Shafiq M, Llorens F, Ferrer I, Andeoletti O et al (2015) Creutzfeldt-Jakob disease subtype-specific regional and temporal regulation of ADP ribosylation factor-1-dependent rho/MLC pathway at pre-clinical stage. J Mol Neurosci 56:329–348
37. Padilla D, Beringue V, Espinosa JC, Andreoletti O, Jaumain E, Reine F, Herzog L, Gutierrez-Adan A et al (2011) Sheep and goat BSE propagate more efficiently than cattle BSE in human PrP transgenic mice. PLoS Pathog 7:e1001319
38. Carimalo J, Cronier S, Petit G, Peyrin JM, Boukhtouche F, Arbez N, Lemaigre-Dubreuil Y, Brugg B et al (2005) Activation of the JNK-c-Jun pathway during the early phase of neuronal apoptosis induced by PrP106-126 and prion infection. Eur J Neurosci 21: 2311–2319
39. Bueler H, Fischer M, Lang Y, Bluethmann H, Lipp HP, DeArmond SJ, Prusiner SB, Aguet M et al (1992) Normal development and behaviour of mice lacking the neuronal cell-surface PrP protein. Nature 356:577–582
40. Kawamoto JC, Barrett JN (1986) Cryopreservation of primary neurons for tissue culture. Brain Res 384:84–93
41. Knusel B, Michel PP, Schwaber JS, Hefti F (1990) Selective and nonselective stimulation of central cholinergic and dopaminergic development in vitro by nerve growth factor, basic fibroblast growth factor, epidermal growth factor, insulin and the insulin-like growth factors I and II. J Neurosci 10:558–570
42. Hotulainen P, Paunola E, Vartiainen MK, Lappalainen P (2005) Actin-depolymerizing factor and cofilin-1 play overlapping roles in promoting rapid F-actin depolymerization in mammalian nonmuscle cells. Mol Biol Cell 16:649–664
43. Arrasate M, Mitra S, Schweitzer ES, Segal MR, Finkbeiner S (2004) Inclusion body formation reduces levels of mutant huntingtin and the risk of neuronal death. Nature 431:805–810
44. Zafar S, Asif AR, Ramljak S, Tahir W, Schmitz M, Zerr I (2014) Anchorless 23-230 PrP(C) interactomics for elucidation of PrP(C) protective role. Mol Neurobiol 49:1385–1399
45. Cory AH, Owen TC, Barltrop JA, Cory JG (1991) Use of an aqueous soluble tetrazolium/formazan assay for cell growth assays in culture. Cancer Commun 3:207–212
46. Zafar S, von Ahsen N, Oellerich M, Zerr I, Schulz-Schaeffer WJ, Armstrong VW, Asif AR (2011) Proteomics approach to identify the interacting partners of cellular prion protein and characterization of Rab7a interaction in neuronal cells. J Proteome Res 10:3123–3135
47. Giorgi A, Di FL, Principe S, Mignogna G, Sennels L, Mancone C, Alonzi T, Sbriccoli M et al (2009) Proteomic profiling of PrP27-30-enriched preparations extracted from the brain of hamsters with experimental scrapie. Proteomics 9:3802–3814
48. Nebl G, Meuer SC, Samstag Y (1996) Dephosphorylation of serine 3 regulates nuclear translocation of cofilin. J Biol Chem 271(42): 26276–26280
49. Gurniak CB, Perlas E, Witke W (2005) The actin depolymerizing factor n-cofilin is essential for neural tube morphogenesis and neural crest cell migration. Dev Biol 278:231–241

50. Giese A, Brown DR, Groschup MH, Feldmann C, Haist I, Kretzschmar HA (1998) Role of microglia in neuronal cell death in prion disease. Brain Pathol 8:449–457
51. Llorens F, Lopez-Gonzalez I, Thune K, Carmona M, Zafar S, Andreoletti O, Zerr I, Ferrer I (2014) Subtype and regional-specific neuroinflammation in sporadic Creutzfeldt-Jakob disease. Front Aging Neurosci 6:198
52. Minamide LS, Striegl AM, Boyle JA, Meberg PJ, Bamburg JR (2000) Neurodegenerative stimuli induce persistent ADF/cofilin-actin rods that disrupt distal neurite function. Nat Cell Biol 2: 628–636
53. Rahman T, Davies DS, Tannenberg RK, Fok S, Shepherd C, Dodd PR, Cullen KM, Goldsbury C (2014a) Cofilin rods and aggregates concur with tau pathology and the development of Alzheimer's disease. J Alzheimers Dis 42:1443–1460
54. Woo JA, Zhao X, Khan H, Penn C, Wang X, Joly-Amado A, Weeber E, Morgan D et al (2015) Slingshot-cofilin activation mediates mitochondrial and synaptic dysfunction via Abeta ligation to beta1-integrin conformers. Cell Death Differ 22:921–934
55. Bernstein BW, Bamburg JR (2010) ADF/cofilin: a functional node in cell biology. Trends Cell Biol 20:187–195
56. Liu L, Li J, Zhang L, Zhang F, Zhang R, Chen X, Brakebusch C, Wang Z et al (2015) Cofilin phosphorylation is elevated after F-actin disassembly induced by Rac1 depletion. Biofactors 41:352–359
57. Cottrell JR, Levenson JM, Kim SH, Gibson HE, Richardson KA, Sivula M, Li B, Ashford CJ et al (2013) Working memory impairment in calcineurin knock-out mice is associated with alterations in synaptic vesicle cycling and disruption of high-frequency synaptic and network activity in prefrontal cortex. J Neurosci 33:10938–10949
58. Zeng H, Chattarji S, Barbarosie M, Rondi-Reig L, Philpot BD, Miyakawa T, Bear MF, Tonegawa S (2001) Forebrain-specific calcineurin knockout selectively impairs bidirectional synaptic plasticity and working/episodic-like memory. Cell 107:617–629
59. Mukherjee A, Soto C (2011) Role of calcineurin in neurodegeneration produced by misfolded proteins and endoplasmic reticulum stress. Curr Opin Cell Biol 23:223–230
60. Gohla A, Bokoch GM (2002) 14-3-3 regulates actin dynamics by stabilizing phosphorylated cofilin. Curr Biol 12:1704–1710
61. Palmer KJ, Watson P, Stephens DJ (2005) The role of microtubules in transport between the endoplasmic reticulum and Golgi apparatus in mammalian cells. Biochem Soc Symp 1-13.
62. Striebel JF, Race B, Carroll JA, Phillips K, Chesebro B (2016) Knockout of fractalkine receptor, Cx3cr1, does not alter disease or microglial activation in prion-infected mice. J Gen Virol